

1 **Running head:** Uncertainty partitioning of forecasts

2

3 **Title:** Using near-term forecasts and uncertainty partitioning to improve predictions of low-
4 frequency cyanobacterial events

5

6 Mary E. Lofton^{1*}, Jennifer A. Brentrup², Whitney S. Beck³, Jacob A. Zwart⁴, Ruchi
7 Bhattacharya⁵, Ludmila S. Brighenti⁶, Sarah H. Burnet⁷, Ian M. McCullough⁸, Bethel G. Steele⁹,
8 Cayelan C. Carey¹⁰, Kathryn L. Cottingham¹¹, Michael C. Dietze¹², Holly A. Ewing¹³, Kathleen
9 C. Weathers¹⁴, Shannon L. LaDeau¹⁵

10

11 ¹Department of Biological Sciences, Virginia Tech, Blacksburg, VA, USA; melofton@vt.edu

12 ^{2a}Department of Biological Sciences, Dartmouth College, Hanover, NH, USA;

13 Jennifer.A.Brentrup@dartmouth.edu

14 ^{3b}Department of Biology and Graduate Degree Program in Ecology, Colorado State University,

15 Fort Collins, CO, USA; whitney.beck@colostate.edu

16 ⁴Integrated Information Dissemination Division, US Geological Survey, Middleton, WI, USA;

17 jzwart@usgs.gov

18 ⁵Legacies of Agricultural Pollutants (LEAP), University of Waterloo, Waterloo, Ontario,

19 Canada; ruchi.bhattacharya@gmail.com

20 ⁶Universidade do Estado de Minas Gerais, Divinópolis, Brazil; ludmilasb@gmail.com

^a Current affiliation: Rubenstein School of Environment and Natural Resources, University of Vermont, Burlington, VT, USA; jennifer.brentrup@uvm.edu

^b Current affiliation: U.S. Environmental Protection Agency, Washington, DC, USA; wbeck1990@gmail.com

21 ⁷Department of Fish and Wildlife Resources, University of Idaho, Moscow, Idaho, USA;

22 shburnet@uidaho.edu

23 ⁸Department of Fisheries and Wildlife, Michigan State University, East Lansing, MI, USA;

24 immccull@gmail.com

25 ⁹Cary Institute of Ecosystem Studies, Millbrook, NY, USA; steeleb@caryinstitute.org

26 ¹⁰Department of Biological Sciences, Virginia Tech, Blacksburg, VA, USA; cayelan@vt.edu

27 ¹¹Department of Biological Sciences, Dartmouth College, Hanover, NH, USA;

28 kathycottingham@esa.org

29 ¹²Department of Earth and Environment, Boston University, Boston, MA, USA; dietze@bu.edu

30 ¹³Environmental Studies, Bates College, Lewiston, ME, USA; hewing@bates.edu

31 ¹⁴Cary Institute of Ecosystem Studies, Millbrook, NY, USA; weathersk@caryinstitute.org

32 ¹⁵Cary Institute of Ecosystem Studies, Millbrook, NY, USA; ladeaus@caryinstitute.org

33

34 *Corresponding author. Address: Department of Biological Sciences, Derring Hall Room 2125,

35 926 West Campus Drive, Mail Code 0406, Blacksburg, VA 24061, USA. Phone: +1-540-231-

36 0788. Fax: +1-540-231-9307. Email: melofton@vt.edu

37

38 This manuscript version is the initial submission for consideration as a research article to

39 *Ecological Applications*. Accepted following peer review on 16 September 2021. Currently in

40 production.

41

42 Declarations of interest: none

43

44 **Abstract**

45 Near-term ecological forecasts provide resource managers advance notice of changes in
46 ecosystem services, such as fisheries stocks, timber yields, or water and air quality. Importantly,
47 ecological forecasts can identify where uncertainty enters the forecasting system, which is
48 necessary to refine and improve forecast skill and guide interpretation of forecast results.
49 Uncertainty partitioning identifies the relative contributions to total forecast variance
50 (uncertainty) introduced by different sources, including specification of the model structure,
51 errors in driver data, and estimation of initial state conditions. Uncertainty partitioning could be
52 particularly useful in improving forecasts of high-density cyanobacterial events, which are
53 difficult to predict and present a persistent challenge for lake managers. Cyanobacteria can
54 produce toxic or unsightly surface scums and advance warning of these events could help
55 managers mitigate water quality issues. Here, we calibrate fourteen Bayesian state-space models
56 to evaluate different hypotheses about cyanobacterial growth using data from eight summers of
57 weekly cyanobacteria density samples in an oligotrophic (low nutrient) lake that experiences
58 sporadic surface scums of the toxin-producing cyanobacterium, *Gloeotrichia echinulata*. We
59 identify dominant sources of uncertainty for near-term (one-week to four-week) forecasts of *G.*
60 *echinulata* densities over two years. Water temperature was an important predictor in calibration
61 and at the four-week forecast horizon. However, no environmental covariates improved over a
62 simple autoregressive (AR) model at the one-week horizon. Even the best fit models exhibited
63 large variance in forecasted cyanobacterial densities and often did not capture rare peak density
64 occurrences, indicating that significant explanatory variables in calibration are not always
65 effective for near-term forecasting of low-frequency events. Uncertainty partitioning revealed
66 that model process specification and initial conditions uncertainty dominated forecasts at both

67 time horizons. These findings suggest that observed densities result from both growth and
68 movement of *G. echinulata*, and that imperfect observations as well as spatial misalignment of
69 environmental data and cyanobacteria observations affect forecast skill. Future research efforts
70 should prioritize long-term studies to refine process understanding and increased sampling
71 frequency and replication to better define initial conditions. Our results emphasize the
72 importance of ecological forecasting principles and uncertainty partitioning to refine and
73 understand predictive capacity across ecosystems.

74

75 **Keywords:** Bayesian model, blooms, dynamic linear model, ecological forecasting, hindcast,
76 lake, oligotrophic, phytoplankton, scums, state-space model, uncertainty partitioning, variance
77 partitioning

78

79

80 **I. Introduction**

81 Near-term ecological forecasts, defined as daily to decadal predictions of the state of
82 ecosystems (Clark et al. 2001, Dietze et al. 2018), can be helpful to resource managers in
83 systems ranging from fisheries stocks to disease outbreaks in protected species populations
84 (Kuikka et al. 2014, Hobbs et al. 2015). For example, near-term forecasts have been used to
85 provide projections for alternate management decisions (Kuikka et al. 2014, Thomas et al. 2018,
86 2020), help managers allot fisheries take quotas (or used to avoid bycatch; Hobday et al. 2019
87 and references therein), and provide advance notice of public safety hazards such as red tides
88 (Stumpf et al. 2009, McGowan et al. 2017). Effective near-term forecasts include fully-specified
89 uncertainty by quantifying the total variance around a prediction and identifying the relative

90 contributions of different sources of uncertainty (Dietze et al. 2018; Box 1).

91 Uncertainty in ecological forecasts may arise from several different sources, including:
92 initial conditions uncertainty, parameter uncertainty, process uncertainty, observation
93 uncertainty, driver or covariate data uncertainty, and random effects uncertainty (Dietze 2017a;
94 Table 1). Partitioning the variance associated with a forecast into these components allows for
95 more targeted efforts to understand and improve forecasts. For example, the dominant
96 contributor to uncertainty in weather forecasts is from initial conditions because the
97 atmosphere's internal instability amplifies even small errors in initial condition estimates and the
98 physical processes controlling weather given a set of current conditions are relatively well-
99 defined (Dietze 2017b). This has directed weather forecasters to prioritize efforts to better
100 measure starting atmospheric conditions (Shuman 1989, Bauer et al. 2015). In contrast, the
101 dominance of process uncertainty in a forecast indicates that researchers need to consider
102 alternative model structures and additional or different explanatory variables to describe the
103 biological or ecological process of interest (Page et al. 2017, Thomas et al. 2018). Formal,
104 standardized uncertainty partitioning can guide improvements to ecological forecasts and
105 ultimately lead to more informed management of natural resources (Bauer et al. 2015, Page et al.
106 2018).

107 Estimating uncertainty has become more common in ecological analyses that generate
108 forecasts (see studies in Table S1 for examples). However, formal uncertainty partitioning that
109 includes all the potential sources of forecast uncertainty is less common and methods are not
110 standardized, making it difficult to compare how different components of uncertainty contribute
111 across ecological systems or among focal state variables. For example, while studies by Gertner
112 et al. 1996, Valle et al. 2009, Wang et al. 2009, and Thomas et al. 2018 (Table S1) all forecast

113 different metrics of forest biomass and productivity, differences in how they estimate and
114 partition uncertainty limit synthetic understanding of the predominance of process structure or
115 estimation of drivers or parameters to uncertainty in forecasts about forest productivity.

116 Forecasting freshwater cyanobacterial dynamics has been a persistent challenge for
117 researchers and water quality managers (Janssen et al. 2019, Rouso et al. 2020), and uncertainty
118 partitioning analysis could help refine and advance forecasting capacity in this system.

119 Cyanobacteria are increasing in many lakes and reservoirs worldwide due to climate and land-
120 use change, posing substantial problems for drinking water managers and other stakeholders
121 (Schindler and Vallentyne 2008, Paerl et al. 2011, Carey et al. 2012b, O’Neil et al. 2012). Many
122 cyanobacterial taxa create toxic or unsightly scums that cause taste and odor problems and clog
123 filters at drinking water treatment plants; consequently, knowing when cyanobacterial density is
124 likely to increase could allow managers to take pre-emptive action to mitigate deleterious water
125 quality effects (van Dolah et al. 2015, Ibelings et al. 2016, Stroom and Kardinaal 2016).

126 However, despite substantial research on drivers of cyanobacterial dominance (e.g., Carey et al.
127 2012b, Paerl and Otten 2013) and recent technological developments permitting high-frequency
128 observations of cyanobacterial density (e.g., Le Vu et al. 2011, Catherine et al. 2012), near-term
129 cyanobacterial abundance model predictions often deviate substantially from observations
130 (Hamilton et al. 2009, Rigosi et al. 2010, Reynolds et al. 2014, Janssen et al. 2019) and few
131 studies have examined forecast uncertainty (Rouso et al. 2020; but see Huang et al. 2013, Page
132 et al. 2017, Massoud et al. 2018). The challenges in forecasting cyanobacteria may be
133 attributable to the rate of cyanobacterial growth relative to the frequency of most sampling
134 campaigns. Cyanobacterial densities can change rapidly on timescales of days to weeks (Dokulil
135 and Teubner 2000, Huisman and Hulot 2005, Rolland et al. 2013, Carpenter et al. 2020), with

136 densities in many lakes remaining relatively low for much of the year and then rapidly increasing
137 from one sample period to the next (e.g., Bormans et al. 2005, Rolland et al. 2013, Carey et al.
138 2014a).

139 Cyanobacterial blooms are often associated with high nutrient levels (Dokulil and
140 Teubner 2000), and so much of the effort to predict cyanobacterial densities has been focused on
141 nutrient-rich lakes (Rousso et al. 2020). As a result, prediction efforts for high-density
142 cyanobacterial events in oligotrophic lakes have lagged behind, and understanding why
143 cyanobacterial densities change over the short term in low-nutrient lakes is especially
144 challenging. However, teasing apart the different sources of uncertainty and their relative
145 importance to cyanobacterial forecast precision may help prioritize research efforts in
146 economically important oligotrophic waterbodies. Increases in the occurrence of high-density
147 cyanobacterial events have been documented in north temperate oligotrophic lakes throughout
148 the United States (Carey et al. 2012a), Canada (Winter et al. 2011), and Europe (Freeman et al.
149 2020), and these increases are often associated with significant economic losses and public
150 health concerns (Dodds et al. 2009, Mueller et al. 2016, Stoddard et al. 2016). High water quality
151 in oligotrophic lakes provides substantial economic benefit through recreational use and high
152 lakeside property values (Wilson and Carpenter 1999, Dodds et al. 2009, Mueller et al. 2016,
153 Stoddard et al. 2016). Moreover, some oligotrophic systems are permitted as drinking water
154 sources with reduced filtration requirements when their water quality meets United States
155 Environmental Protection Agency (U.S. EPA) standards, thereby reducing water treatment costs
156 (U.S. EPA 1991, Kauffman 2016, Ravindranath et al. 2016).

157 Prior studies provide several hypotheses for what environmental drivers likely trigger
158 cyanobacterial growth or accumulation of cyanobacterial surface scums, including: increased

159 growth at higher temperatures (Paerl and Huisman 2008, Hamilton et al. 2009); light-induced
160 triggering of cell germination and growth (Roelofs and Oglesby 1970, Karlsson-Elfgren et al.
161 2004); more recruitment of dormant cells from the sediment and/or dilution of surface water
162 cyanobacterial density due to water column mixing, which can occur due to temperature
163 changes, precipitation events, or wind (Jennings et al. 2012, Carey et al. 2014, de Eyto et al.
164 2016, Kuha et al. 2016); greater incidence of surface scums during periods of stronger thermal
165 stratification (Carey et al. 2012b); and aggregation of cells or colonies in nearshore zones by
166 wind (Roelofs and Oglesby 1970, Cyr 2017). The development of forecast models with
167 uncertainty partitioning is needed to compare and evaluate these hypotheses in a predictive
168 framework.

169 While there are a variety of techniques that can be used to develop forecast models with
170 partitioned uncertainty, Bayesian state-space models are particularly suitable (Clark 2007, Hobbs
171 and Hooten 2015, Dietze 2017a). State-space models focus on estimating the true, latent state of
172 the system by explicitly accounting for observation and process uncertainty. These dynamic
173 models are structured so that each modeled latent state is a function of the previous latent state,
174 independent of observations at other time points (Hobbs and Hooten 2015, Dietze 2017a; Fig. 1).
175 Bayesian state-space models use distributions rather than fixed values to represent all unknown
176 values, including parameters, initial conditions, and as-yet-unobserved future values for driver
177 variables, allowing for quantification of uncertainty associated with each of these components
178 and missing data.

179 We developed and evaluated a suite of Bayesian state-space models with different
180 structures and tested different environmental variables hypothesized to be important in driving
181 cyanobacterial density, including water temperature, thermal stability, wind, and light. We

182 calibrated each model to weekly cyanobacterial densities measured from 2009-2014 in Lake
183 Sunapee, NH, USA, an oligotrophic lake that exhibits variable densities of the toxin-producing
184 cyanobacterium *Gloeotrichia echinulata*. We then generated hindcasts (defined in Table 1) of
185 cyanobacterial density for 2015-2016. We assessed and conducted uncertainty partitioning of our
186 hindcasts to address the following questions: A) Which model structures and environmental
187 covariates best predict oligotrophic lake cyanobacterial density over one to four week forecast
188 horizons? B) What are the dominant sources of uncertainty in oligotrophic lake cyanobacterial
189 forecasts? and C) How do the relative contributions of different sources of uncertainty vary
190 among models with differing complexity and environmental covariates? We discuss how our
191 results inform future efforts to forecast oligotrophic lake cyanobacterial density and relate to
192 patterns of predictive uncertainty observed in other ecosystems.

193

194

195 **II. Methods**

196 *Focal cyanobacterium*

197 *Gloeotrichia echinulata* is a colonial, filamentous cyanobacterium commonly found in
198 oligotrophic north temperate lakes in the United States, Canada, and Europe (Karlsson-Elfgren et
199 al. 2005, Winter et al. 2011, Carey et al. 2012a, Freeman et al. 2020). *G. echinulata* is capable of
200 forming surface scums and producing toxins (Karlsson-Elfgren et al. 2005, Carey et al. 2012a).
201 Occurrence of *G. echinulata* surface scums in oligotrophic north temperate lakes has been
202 increasing in recent decades (Carey et al. 2008, 2012a, Winter et al. 2011), motivating
203 researchers to improve understanding and prediction of *G. echinulata* density in these
204 ecosystems. While nutrients are often a driver of cyanobacterial growth in eutrophic lakes

205 (Dokulil and Teubner 2000), current understanding of dynamics in oligotrophic systems suggests
206 that other environmental drivers may be important for determining *G. echinulata* densities
207 (Roelofs and Oglesby 1970, Karlsson-Elfgren et al. 2004, Carey et al. 2014, Cyr 2017).

208

209 *Study site*

210 We sampled *G. echinulata* surface abundance and collected environmental data weekly in
211 May-October from 2009-2016 at two nearshore sites in Lake Sunapee, NH, USA, a recreational
212 lake with high property values that also serves as a public drinking water supply (Fig. 2). Lake
213 Sunapee is a large, oligotrophic lake (lat 43°24'N, long 72°2'W, max. depth = 33.7 m, surface
214 area = 16.69 km², volume = 1.94 × 10 m³, mean depth = 11.6 m, Lake Sunapee Protective
215 Association (LSPA), unpublished data). High-nutrient (eutrophic) lakes can have total
216 phosphorus (TP) concentrations ≥ 24 µg L⁻¹ and total nitrogen (TN) concentrations ranging from
217 ~400-1600 µg L⁻¹ (Carlson 1977, Carlson and Simpson 1996, Gibson et al. 2000). Mean TP
218 concentration in the surface waters of Lake Sunapee between 2009-2016 was 6.3 ± 1.7 µg L⁻¹
219 (mean ± 1 S.D.), and mean Secchi depth was 6.6 ± 0.6 m (LSPA, unpub. data). Mean TN
220 concentration from 2009-2012 at our study site was 172 ± 25 µg L⁻¹ (Cottingham 2020). Lake
221 Sunapee typically thermally stratifies from June-September with a mean thermocline depth of 7-
222 9 m from 2009-2016. The watershed (~107 km² not including lake surface area) is 80% forested
223 but shoreline development has been increasing in recent decades (Cobourn et al. 2018).

224 Our research team began a weekly *G. echinulata* monitoring program at two sampling
225 sites in collaboration with the Lake Sunapee Protective Association (LSPA) in 2005 (Carey et al.
226 2008, 2014b). Our focal sampling site for this study (Site 1; Fig. 2) was chosen because it
227 frequently exhibits high densities of *G. echinulata*. We used data from the second nearshore site

228 (Site 2) only to generate informed priors for *G. echinulata* observation error and nearshore water
229 temperature and these data were not included in any hindcasting analyses. We focused our
230 analyses on 2009-2016 for this study because those years had at least 20 weeks of sampling data
231 (Cottingham et al. 2020a); however, during our eight-year study period there were six missing
232 weekly *G. echinulata* observations, four of which occurred during the 2015-2016 hindcasting
233 period.

234

235 *G. echinulata* data collection and sample processing

236 *G. echinulata* surface abundance at both nearshore sites was sampled each week in the
237 top 1 m of the water column by combining two vertical tows from 1 m to the surface using a 30
238 cm diameter, 80 µm mesh plankton net (Wildlife Supply Co., Yulee, Florida). *G. echinulata*
239 were transferred from the net and preserved in opaque plastic bottles using Lugol's iodine (Carey
240 et al. 2014). Total *G. echinulata* samples were counted using a Leica MZ12 dissecting
241 microscope (Leica, Buffalo Grove, Illinois). Density was quantified according to the number of
242 colonies and filament bundles (immature, developing colonies) per liter rather than biovolume
243 following protocols used in previous studies of *G. echinulata* (Roelofs and Oglesby 1970,
244 Barbiero and Welch 1992, Karlsson-Elfgren et al. 2005). We then converted abundance to
245 density by dividing the total number of colonies and filament bundles in each sample by the
246 volume of water sampled by the plankton net (Carey et al. 2014b). All data are publicly available
247 through the Environmental Data Initiative repository (Cottingham et al. 2020a, 2020b, LSPA et
248 al. 2020a, 2020b; Lofton et al. 2020).

249

250

251 *Environmental driver data*

252 To capture the effect of temperature on *G. echinulata* growth, water temperature was
253 monitored hourly using Onset loggers at our nearshore sampling sites (Sites 1 and 2; Fig. 2;
254 Cottingham et al. 2020b). Growing degree days (GDD), a measure of heat accumulation during
255 the growing season, were calculated using these water temperatures for each day when *G.*
256 *echinulata* was sampled. To investigate effects of thermal stratification on *G. echinulata* surface
257 density, water temperature profiles from the Global Lake Ecological Observatory Network
258 (GLEON) buoy, deployed in the lake by the LSPA since 2007 (Site 3), were used to calculate
259 Schmidt stability, a measure of thermal stratification strength that indicates the amount of energy
260 required to homogenize temperature across the water column (Idso 1973, LSPA et al. 2020b). To
261 examine whether wind could drive nearshore aggregation of *G. echinulata* colonies, wind data
262 from the LSPA/GLEON buoy (Site 3) were aggregated from minute and hourly scales,
263 respectively, to calculate daily summary statistics (LSPA et al. 2020a). Solar radiation data from
264 the North American Land Data Assimilation System Phase 2 (NLDAS-2) forcing dataset
265 (<https://ldas.gsfc.nasa.gov/nldas>; Lofton et al. 2020) and photosynthetically active radiation
266 (PAR) data from the LSPA/GLEON buoy (LSPA et al. 2020a) were similarly aggregated to
267 determine whether light was an important predictor of *G. echinulata* density. Finally, we
268 calculated summary statistics of daily precipitation data from the Parameter-elevation
269 Relationships on Independent Slopes Model (PRISM) model (<http://www.prism.oregonstate.edu>;
270 Lofton et al. 2020) to examine the effect of storm events and subsequent water column mixing
271 on *G. echinulata* pelagic populations (see Text S1 for further information on environmental data
272 processing).

273

274 *Selection of environmental covariates for Bayesian models*

275 We performed a standardized selection process to determine which potential
276 environmental drivers of *G. echinulata* density to include in Bayesian state-space models (Text
277 S2). We examined associations between natural log-transformed *G. echinulata* density from
278 2009-2014 (calibration period) and 82 summary statistics of candidate environmental covariates
279 identified as potential drivers in previous studies (Roelofs and Oglesby 1970, Karlsson-Elfgren
280 et al. 2004, Paerl and Huisman 2008, Hamilton et al. 2009, Carey et al. 2012b, 2014, Jennings et
281 al. 2012, de Eyto et al. 2016, Kuha et al. 2016, Cyr 2017). We used Spearman correlations to
282 prioritize inclusion in our Bayesian models (Text S2). The full list of covariate summary
283 statistics is in Table S2. This approach identified eight drivers for further evaluation (Table 2):
284 daily minimum water temperature on the sampling day (MinWaterTemp), daily minimum water
285 temperature with a one-week lag (MinWaterTempLag), seven-day moving average of water
286 temperature (WaterTempMA), weekly difference in median Schmidt stability (Δ Schmidt), daily
287 maximum Schmidt stability with a one-week lag (SchmidtLag), daily mean of a wind direction
288 indicator variable with a two-day lag (WindDir; see Text S1 for details on wind indicator
289 variable calculation), growing degree days (GDD), and daily sum of precipitation (Precip).

290

291 *Development of Bayesian state-space models*

292 A suite of Bayesian state space models were fit to data collected from Site 1 and
293 increased in complexity from a random walk with no covariates (intercept model) to models
294 containing one or two of the eight prioritized driver variables (Fig. 3; Table 2). We calibrated
295 each model over a 6-year period from 2009-2014, assessed model performance during a two-year
296 hindcasting period of 2015-2016, and then conducted uncertainty partitioning. We investigated

297 whether sequential increases in model complexity translated to changes in the relative
298 contributions of different uncertainty sources to total hindcast uncertainty, increases in skill of *G.*
299 *echinulata* density hindcasts, or both (Fig. 3; Table 2).

300 We assessed hindcast skill of the twelve models including environmental covariates
301 compared to two baseline models: first, a model with a random walk process and an informed
302 prior for observation error developed using data from Site 2 (RW model; Fig. 3; Text S3), and
303 second, a linear autoregressive process model with a single lag (AR model; Fig. 3; Table 2). We
304 also assessed a random walk model with a random year effect as a possible baseline model but
305 determined during model calibration that the estimated year effect was not substantially different
306 from 0 in any year (Table S3); as a result, we did not include a random year effect in subsequent
307 models. We next incorporated a single environmental covariate into the linear AR(1) process
308 model based on our environmental covariate selection process (MinWaterTemp,
309 MinWaterTempLag, WaterTempMA, Δ Schmidt, SchmidtLag, WindDir, Precip, and GDD). The
310 influence of GDD was visibly non-linear in our preliminary analyses (Fig. S1) and thus, a
311 quadratic term was included in the model to evaluate GDD influence on *G. echinulata* growth.

312 We subsequently developed two-covariate models based on the performance of the
313 single-covariate models during the hindcasting validation period (Schmidt+Temp,
314 Schmidt+Precip, Temp+Precip, Precip+GDD). Finally, following observations that model
315 ensembles can provide more skilled predictions than a single model even when some ensemble
316 members are low-performing (Johansson et al. 2019), we generated a simple, unweighted model
317 ensemble to determine if it could out-perform our individual models (see Text S4 for model
318 ensemble details).

319

320 *Calibration using 2009-2014 data*

321 We calibrated each Bayesian state-space model to observed weekly data collected in
322 2009-2014 using the R packages *rjags* and *runjags* (*rjags* v.4-8, *runjags* v. 2.0.4-2, Denwood
323 and Plummer 2019, Plummer et al. 2019) in the R statistical environment (R version 4.0, R Core
324 Development Team, 2020). Models were structured as an annual loop for 20 weeks per year,
325 with each season extending from the last week in May to the first week in October. We natural
326 log-transformed *G. echinulata* densities and standardized all covariates using Z-scores to
327 facilitate model convergence. We ran three Markov chain Monte Carlo (MCMC) chains for each
328 model, with an adaptation period of 5,000 iterations, a burn-in of 10,000 iterations, and a sample
329 size of 50,000 iterations, which we thinned to 7,500 samples for hindcasting and model
330 assessment. We evaluated convergence using the potential scale reduction factor of the Gelman-
331 Rubin statistic, sometimes referred to as \hat{R} , where a value approaching 1 indicates that the model
332 has converged well on a parameter estimate both within and among MCMC chains (Table S4;
333 Table S5). Missing data occurred for several of our candidate environmental drivers, so NA
334 values were imputed using a missing data model with a Gaussian prior with mean and variance
335 of observations from the same week across the calibration period (2009-2014).

336

337 *Hindcasting validation using 2015-2016 data*

338 To validate our Bayesian state-space models, we conducted one-week-ahead and four-
339 week-ahead hindcasts of *G. echinulata* density in 2015-2016 using each of the fourteen models.
340 We assimilated data by iteratively adding one week of data to our model input dataset and re-
341 running our Bayesian models in *runjags* to update parameter calibrations and initial conditions.
342 The posterior output of each re-calibrated model was then used to produce hindcasts at one and

343 four weeks into the future. We hindcasted “future” driver data for each environmental covariate
344 using data observations from 2009-2014 for the 2015 hindcasts and from 2009-2015 for the 2016
345 hindcasts. These historical driver timeseries were resampled with replacement for each of the
346 7,500 hindcast model iterations to account for week-to-week autocorrelation in driver data. As
347 hindcasts were running, driver data from 2015-2016 were assimilated along with *G. echinulata*
348 observations and thereby used to update posteriors throughout the hindcasting period.

349 Our primary criterion for hindcast model selection was based on predictive loss,
350 calculated using the root mean square error (RMSE) of predictions and the variance of the
351 predictive interval (defined in Table 1) via the following equation:

$$352 \quad \text{Predictive loss} = \sqrt{RMSE^2 + \text{predictive interval variance}} \quad \text{eqn. 1}$$

353 The model with the smallest predictive loss at a particular forecast horizon indicates the best-
354 performing model at that horizon (Gelfand and Ghosh 1998). We further compared models by
355 subtracting the predictive loss of the best-performing model from the predictive loss of all other
356 models to calculate change in predictive loss (Δ PL), with smaller Δ PL indicating better-
357 performing models. We also calculated the standard deviation of the predictive interval
358 (predictive S.D.), the percent of observations falling within the 95% predictive interval
359 (coverage), the mean difference between median predicted and observed values (bias), and the
360 difference in weeks between when maximum *G. echinulata* density was observed during the
361 hindcasting period and when each model predicted maximum *G. echinulata* density (peak
362 timing; Table 3).

363

364

365

366 *Uncertainty partitioning of 2015-2016 hindcasts*

367 We conducted uncertainty partitioning of our 2015-2016 cyanobacterial density hindcasts
368 using a one-at-a-time ahead approach, where all sources of uncertainty were initially held at
369 fixed values and then sequentially added back into the hindcasts. For example, all model
370 parameter values were initially set to the mean of the posterior distribution of the calibrated
371 model for all 7,500 hindcasting iterations; then, when we wanted to add parameter uncertainty to
372 our hindcasts, we allowed parameter values to be drawn from the full posterior distribution,
373 resulting in a variety of possible parameter values and subsequent estimation of uncertainty in
374 those parameters. We added sources of uncertainty to our hindcasts in the following order: initial
375 condition uncertainty, parameter uncertainty, driver data uncertainty, and process uncertainty.
376 The order of uncertainties is important to specify as different sources of uncertainty can interact
377 with each other. We were then able to calculate the relative contribution of each uncertainty
378 source to total hindcast variance based on the incremental increase in variance as each source of
379 uncertainty was added. Not all models included all the potential sources of uncertainty (e.g., the
380 random walk model does not have driver data uncertainty because it does not include any
381 environmental covariates).

382 Observation uncertainty is not included in our partitioning results because it does not
383 propagate and therefore does not affect our uncertainty about the latent state of the system
384 (Dietze 2017). However, to examine the relative importance of observation error in our study
385 system, we assessed the estimated value of τ_{obs} , which is the precision ($\frac{1}{S.D.^2}$) of the normal
386 distribution used to fit *G. echinulata* latent states to *G. echinulata* observations in the data model
387 component of our Bayesian state-space models (Fig. 1). We also examined the increase in
388 variance between our 95% credible interval (CI) and our 95% predictive interval (PI; CI and PI

389 are defined in Table 1).

390 All code used for data processing, model calibration and validation, uncertainty
391 partitioning, and assessment of hindcast output are publicly available on the GLEON Github
392 repository (https://github.com/GLEON/Bayes_forecast_WG/tree/eco_apps_release;
393 DOI:10.5281/zenodo.3878781).

394

395

396 **III. Results**

397 *Variability in G. echinulata abundance*

398 Median *G. echinulata* density during the entire study period from 2009-2016 was $0.25 \pm$
399 8.2 colonies L^{-1} (median ± 1 S.D.; Fig. 4). During the model calibration period (2009-2014), *G.*
400 *echinulata* density ranged from an annual maximum density of 1.2 colonies L^{-1} in 2012 to 81.6
401 colonies L^{-1} in 2013. Notably, while the calibration years included two periods of high *G.*
402 *echinulata* density with visible surface scums (42.1 colonies L^{-1} in August 2010 and 81.4
403 colonies L^{-1} in September 2013), maximum density during the 2015-2016 hindcasting validation
404 period was 14.1 colonies L^{-1} (Fig. 4). Temporal variability in environmental drivers of *G.*
405 *echinulata* density included in state-space models is reported in Text S5 and Figures S2 – S9.

406

407 *Models of G. echinulata growth*

408 *G. echinulata* growth was dependent on *G. echinulata* density at the previous timestep, as
409 indicated by a converged coefficient value ranging from 0.63 to 0.76 ± 0.06 to 0.10 for the
410 AR(1) term across models (Table S4). Parameter estimates from calibrated models indicated that
411 *G. echinulata* growth was positively associated with increases in water temperature, high

412 Schmidt stability, and a higher daily proportion of wind blowing towards the focal nearshore site
413 (see Table S4; Table S5 for model coefficient values). The coefficient on the quadratic term for
414 growing degree days based on water temperature (GDD) converged at -0.59 ± 0.17 (Table S5),
415 indicating that increases in GDD at high values (i.e., late in the sampling season) were associated
416 with decreasing *G. echinulata* growth.

417 Some variables that seemed promising based on our covariate selection protocol had
418 estimated model coefficients close to 0 in calibrated state-space models (Precip, Δ Schmidt),
419 indicating a limited effect on *G. echinulata* growth. The daily sum of precipitation (Precip) and
420 weekly difference in median Schmidt stability (Δ Schmidt) model coefficients did not differ from
421 zero (Table S5). Model coefficient values did not substantially change when environmental
422 covariates were combined in two-covariate models (Schmidt+Temp, Schmidt+Precip,
423 Temp+Precip, Precip+GDD, Table S5).

424

425 *Environmental drivers no better than AR model at one-week-ahead hindcasts*

426 All single and two-covariate models and the AR model had improved performance over
427 the null RW model for one-week-ahead hindcasts based on predictive loss. Three models (AR,
428 Δ Schmidt, and Precip) had a predictive loss of $2.25 \ln(\text{colonies L}^{-1})$ and were also comparable in
429 terms of RMSE, coverage, and bias (Table 3; Fig. 5; models not shown in Fig. 5 can be found in
430 Fig. S10, S11). Other environmental covariates that had non-zero model coefficients ($\hat{\beta}$
431 parameters; Table S5), such as the water temperature covariates, SchmidtLag, and WindDir,
432 were not good predictors of *G. echinulata* densities at the one-week horizon (Table 3).

433 No model correctly predicted the week or magnitude of peak *G. echinulata* density for
434 the 2015-2016 hindcasting period (10 September 2015) at the one-week horizon; however, the

435 best-performing AR model was able to predict when peak density occurred with only a one week
436 lag after the observed peak (Table 3).

437

438 *Water temperature models more skilled than AR at four-week forecast horizon*

439 Models containing water temperature covariates out-performed the AR model at the four-
440 week horizon (Table 3; Fig. 6; models not shown in Fig. 6 may be found in Fig. S12, S13). The
441 three best-performing models at the four-week horizon were MinWaterTempLag,
442 WaterTempMA, and Schmidt+Temp, all with a predictive loss of 2.42 $\ln(\text{colonies L}^{-1})$. Other
443 models containing water temperature covariates (MinWaterTemp, GDD, Temp+Precip,
444 Precip+GDD) also performed relatively well at the four-week horizon, all with $\Delta\text{PL} = 0.01$
445 $\ln(\text{colonies L}^{-1})$. Models containing water temperature covariates tended to have lower bias and
446 lower predictive S.D. than other models at the four-week horizon; however, the reduction in
447 predictive S.D. corresponded to a loss in coverage (Table 3).

448 Despite the improvement of water temperature models over the AR model, no examined
449 model successfully predicted the timing of peak *G. echinulata* density at the four-week horizon,
450 and all models missed the peak by 12 or 14 weeks. Given the structure of our models (seasonal
451 for-loop), this means that models missed the 10 September 2015 peak altogether (Fig. 6).

452 The unweighted model ensemble was not among the top-performing models at either the
453 one-week or four-week forecast horizon, with a ΔPL of 0.05 $\ln(\text{colonies L}^{-1})$ at the one-week
454 horizon and 0.09 $\ln(\text{colonies L}^{-1})$ at the four-week horizon (Table 3; Text S4).

455

456

457

458 *Process uncertainty dominates hindcast credible intervals*

459 Process uncertainty represented the largest proportion of uncertainty in the credible
460 interval for all models. The proportion of the variance attributed to process uncertainty increased
461 with hindcast horizon, largely due to a reduction in initial conditions uncertainty (Fig. 7; models
462 not shown in Fig. 7 can be found in Fig. S14). Neither increases in model structural complexity
463 or differences in model covariates substantially decreased the proportional contribution of
464 process uncertainty (Fig. 8). The mean contribution of process uncertainty across the hindcasting
465 period ranged from 73% of hindcast uncertainty in the RW model to 81% in the
466 MinWaterTempLag model for one-week-ahead hindcasts, and from 83% in the SchmidtLag
467 model to 93% in the AR model for four-week-ahead hindcasts. However, the relative
468 contribution of process uncertainty to total hindcast uncertainty did vary across the hindcasting
469 period for individual models (mean, minimum, and maximum contributions of all uncertainty
470 sources during 2015-2016 can be found in Tables S6-S7). Excluding the RW and AR models,
471 whose credible intervals became almost completely comprised of process error as the forecast
472 horizon progressed, process error was sometimes as low as 54% (Δ Schmidt, SchmidtLag,
473 WindDir) or as high as 96% (Δ Schmidt, Precip) for one-week-ahead hindcasts, and as low as
474 73% (SchmidtMaxLag) or as high as 95% (Precip) for four-week-ahead hindcasts.

475 The second largest component of uncertainty in hindcasts was due to initial conditions
476 estimation, although this source of uncertainty quickly declined to negligible levels by the four-
477 week-ahead forecast horizon for all models (Fig. 7; Fig. 8). Averaged across the hindcasting
478 period, initial conditions uncertainty contributed from 13% (MinWaterTempLag;
479 Schmidt+Temp) to 27% (RW) of the uncertainty for one-week-ahead hindcasts but comprised
480 only from 1 % to 9% of total uncertainty for four-week ahead hindcasts. Initial conditions

481 uncertainty was largest (30-43% of total uncertainty) for one-week-ahead hindcasts following a
482 week with a missing *G. echinulata* observation (Fig. S15a).

483 Parameter and driver error had negligible contributions to total hindcast uncertainty for
484 both one-week-ahead and four-week-ahead hindcasts (Fig. 7; Fig. 8; Fig. S14 and Tables in
485 Supplemental Material).

486

487 *Observation uncertainty in 95% PI*

488 Observation uncertainty was a substantial component of uncertainty for all models and
489 τ_{obs} ranged from 1.72 to 1.89 ± 0.35 to $0.38 \ln(\text{colonies L}^{-1})^{-2}$ across models. This corresponds to
490 a standard deviation of $\sim 0.75 \ln(\text{colonies L}^{-1})$ or $\sim 2.1 \text{ colonies L}^{-1}$, which is large considering
491 that median *G. echinulata* density during the hindcasting period was $0.56 \pm 2.9 \text{ colonies L}^{-1}$.
492 These relatively large estimates of observation uncertainty contributed to an average increase of
493 $0.94 \ln(\text{colonies L}^{-1})$ in the 95% predictive interval (PI) over the 95% credible interval (CI; mean
494 range $4.88 \pm 0.40 \ln(\text{colonies L}^{-1})$) across all models for one-week-ahead hindcasts (Fig. 5). The
495 difference in PI was higher for the four-week-ahead hindcasts, with a $1.16 \ln(\text{colonies L}^{-1})$
496 increase over the 95% CI (mean CI range $5.61 \pm 1.11 \ln(\text{colonies L}^{-1})$) across all models (Fig. 6).
497 Again considering the relatively low density of *G. echinulata* during our hindcasting period,
498 these 95% PI – 95% CI range differences translate to a large contribution of observation
499 uncertainty to predicted *G. echinulata* densities (95% PI – 95% CI range differences of 2.56
500 colonies L^{-1} at the one-week horizon and 3.12 colonies L^{-1} at the four-week horizon).

501

502

503

504 IV. Discussion

505 Understanding ecological systems to better forecast future events is a critical challenge
506 for managing resources and public health. Use of standardized ecological forecasting approaches
507 provides a much-needed framework for prioritizing research efforts to meet this challenge. While
508 there are numerous hypotheses and studies linking environmental drivers to the *G. echinulata*
509 surface scums that challenge water quality management in oligotrophic lakes (e.g., Roelofs and
510 Oglesby 1970, Istvánovics et al. 1993, Hyenstrand et al. 2000, Karlsson-Elfgren et al. 2005,
511 Carey et al. 2014, Napiórkowska-Krzebietke and Hutorowicz 2015), few have fully evaluated the
512 predictive influence of these environmental variables. We calibrated models to evaluate how
513 well environmental variables that had previously been associated with cyanobacterial density
514 explain changes in density over near-term timescales and evaluated each model for forecast skill.
515 We demonstrate that significant explanatory variables in calibration or best-fit models are not
516 necessarily effective driver variables in near-term ecological forecasts, and that driver variables
517 that may adequately capture low densities may not successfully predict rare high-density events.
518 The dominance of process and initial conditions uncertainty in our forecasts emphasizes that *G.*
519 *echinulata* densities are likely a product of both growth and movement of colonies, that spatial
520 and temporal misalignment of driver data and density observations are ongoing challenges in this
521 forecasting system, and that imperfect observation of both *G. echinulata* density and
522 environmental covariates substantially affect forecast skill.

523 Of all the environmental covariates we examined, water temperature metrics were
524 important in both calibration and hindcast models and may be a promising suite of drivers for
525 predicting *G. echinulata* density. Both lagged and moving average measures of water
526 temperature (MinWaterTempLag, WaterTempMA) were positively associated with changes in

527 *G. echinulata* density and more skilled than the baseline AR model in hindcasting *G. echinulata*
528 density at the four-week horizon. This is consistent with studies demonstrating that
529 cyanobacteria benefit from warmer temperatures (e.g., Paerl and Huisman 2008, Carey et al.
530 2012b), that water temperature is a good predictor of cyanobacterial density (Rousso et al. 2020),
531 and that antecedent conditions can affect cyanobacterial growth and phytoplankton community
532 structure (Bormans et al. 2005, Madgwick et al. 2006). Our results further suggest that a
533 minimum water temperature predictor (MinWaterTempLag) may be useful for forecasting *G.*
534 *echinulata* density, which agrees with findings from a previous study examining predictors of
535 *Lyngbya majuscula* blooms in an Australian bay (Hamilton et al. 2009). However, we were
536 unable to identify any environmental covariates that improved *G. echinulata* density predictions
537 over the AR model at the one-week horizon, suggesting that water temperature is likely not
538 adequate to forecast cyanobacterial densities at this time scale.

539 Process uncertainty dominated hindcast uncertainty across all models. Neither increases
540 in model structural complexity nor differences in model covariates substantially decreased the
541 proportional contribution of process uncertainty to forecast uncertainty. The predominance of
542 process uncertainty, coupled with low parameter uncertainty (Fig. 8), indicates a substantial need
543 for research to better understand how and why *G. echinulata* densities change. Some of the
544 environmental covariates we explored may sufficiently explain weekly differences in frequently-
545 observed low densities but none of the models we calibrated had skill at forecasting peak
546 abundances, which appeared and declined suddenly. In theory, it is possible that *G. echinulata*
547 dynamics are dominated by stochasticity (e.g., Carpenter et al. 2020), in which case
548 improvement to model structure would not effectively reduce process uncertainty. However, our
549 results suggest that a process model more aligned with the biology of the focal cyanobacterium,

550 as well as more frequent sampling events, could be promising avenues for model development to
551 reduce process uncertainty and improve forecast skill.

552 The low-frequency surface scum events in Lake Sunapee likely result from the compound
553 effects of cyanobacterial population growth in the water column, recruitment of dormant cells
554 from the sediments, movement of colonies within the lake, and accumulation on the lake surface
555 (Roelofs and Oglesby 1970, Karlsson-Elfgren et al. 2005, Carey et al. 2014, Cyr 2017). Each of
556 these may be best predicted by different drivers at different temporal or spatial scales, and many
557 more years of data are likely needed to identify significant predictors of these low-frequency,
558 high-density cyanobacterial growth events. Absent the possibility of data-driven models to
559 predict low-frequency events, more mechanistic process structure in the forecasting model is
560 needed. Changes in the relative importance of driver and process uncertainty in our hindcasts
561 may elucidate when during the season currently unaccounted-for ecological processes are
562 important and how we could better align environmental driver and *G. echinulata* density
563 sampling in future studies. For example, one of the best-performing models at the four-week
564 horizon (MinWaterTempLag) exhibited low driver uncertainty but high process uncertainty
565 during the last five weeks of the 2015 sampling season (Fig. S16). This suggests that *G.*
566 *echinulata* were responding to variables other than water temperature and a careful examination
567 of other environmental conditions during this period could illuminate additional ecological
568 processes that should be included in forecasting models. Further, incorporating more mechanistic
569 representations of explanatory variables that were significant during model calibration but not
570 skilled at forecasting, such as wind direction and thermal stratification (SchmidtLag), might help
571 constrain process uncertainty. Models including both temperature-dependent growth rate
572 equations and a process representation of the effect of thermal stratification on surface scum

573 formation or of colony transport via wind-driven mixing (e.g., Wallace et al. 2000, Ndong et al.
574 2017, Cyr 2017) might generate better forecasts. A more complex mechanistic model could also
575 include additional life history stages of *G. echinulata* beyond vegetative growth in the water
576 column. For example, it is well-documented that recruitment from the sediments to the pelagic
577 zone is an important life stage for *G. echinulata*, potentially contributing 4-40% of the water
578 column population each week (e.g., Barbiero and Welch 1992, Carey et al. 2014b).

579 While the contribution of driver data uncertainty (accuracy of driver measurements and
580 forecasts) to our hindcasts was small, spatial mismatches between driver data and response
581 variable data may also contribute to process uncertainty. Thus, the inclusion of more nearshore
582 site variables, rather than variables collected in the deep-water pelagic zone, might reduce
583 process uncertainty by better characterizing the effect of environmental drivers on localized
584 nearshore processes. For example, we did not consider nearshore nutrient concentrations. *G.*
585 *echinulata* can both fix nitrogen and sequester excess phosphorus in the sediments before
586 recruiting to the water column, thereby providing its own nutrients for pelagic growth (Barbiero
587 and Welch 1992, Cottingham et al. 2015); moreover, our study lake has very low nitrogen and
588 phosphorus concentrations. However, it is possible that nearshore nutrient concentrations could
589 have an effect on *G. echinulata* growth. In addition, local site variables have been found
590 important in driving benthic recruitment (Carey et al. 2014), so inclusion of more nearshore
591 drivers could be a complementary approach to including benthic recruitment in models.

592 Forecast skill in this system could also be improved by refining our estimates of initial
593 conditions. In particular, both total hindcast variance and the proportional contribution of initial
594 condition uncertainty exhibited large increases immediately after missing *G. echinulata* density
595 observations, and this increase perpetuated through the four-week horizon (Fig. S11). This

596 suggests that increasing the spatial or temporal frequency of observations could improve forecast
597 skill (e.g., Fox et al. 2018), as cyanobacterial densities can be spatially heterogeneous (Franks
598 1997, Serizawa et al. 2008, Wynne and Stumpf 2015) and change quickly on short timescales
599 (Dokulil and Teubner 2000, Huisman and Hulot 2005, Rolland et al. 2013). Because sampling
600 and counting *G. echinulata* is labor-intensive, increasing observational frequency might
601 necessitate assimilating other measures of cyanobacterial abundance into forecasts, such as
602 fluorescence-based biomass measurements (e.g., Catherine et al. 2012) and spectrophotometric
603 pigment analysis (e.g., Küpper et al. 2007, Thrane et al. 2015). Furthermore, as phytoplankton
604 counts are notoriously variable (Rott et al. 2007, Vuorio et al. 2007), increased spatio-temporal
605 sampling frequency and incorporation of measures of cyanobacterial abundance besides counts
606 might constrain the high observation uncertainty in *G. echinulata* density data, thereby
607 improving comparisons of models to data. However, before investing in costly increased *in-situ*
608 monitoring, the potential benefit of increased sampling effort could be determined through
609 simulated data experiments exploring how different sampling techniques and frequencies affect
610 forecast precision (following Dietze 2017a).

611 Our uncertainty partitioning results from oligotrophic lake cyanobacterial density
612 hindcasts have some commonalities with other uncertainty partitioning efforts, contributing
613 insight into the dominant sources of uncertainty across near-term forecasts in ecological systems.
614 Our hindcasts were dominated by process uncertainty and emphasize the need for research to
615 better understand the ecology of phytoplankton density changes in nutrient-poor systems. Similar
616 results have been reported for ecological forecasts at decadal and multi-decadal timescales
617 predicting variables ranging from forest biomass and productivity (Thomas et al. 2018) to
618 vertebrate species distributions (Diniz-Filho et al. 2009, Watling et al. 2015). In addition, our

619 finding that initial conditions uncertainty is an important contributor to forecast uncertainty is
620 consistent with terrestrial carbon forecasts at the annual scale (Fox et al. 2018) and lake
621 chlorophyll-*a* forecasts at the weekly scale (Huang et al. 2013). However, several other aquatic
622 and terrestrial forecasts that could leverage good process understanding found that driver data
623 uncertainty dominated ecological forecasts (e.g., Mbogga et al. 2010, Dietze 2017b, Ouellet-
624 Proulx et al. 2017, Jiang et al. 2018, Thomas et al. 2020). Across ecosystems, a skillful process
625 model and correspondingly low process uncertainty are likely prerequisites for other forms of
626 uncertainty, such as driver data uncertainty, to dominate.

627 Developing forecasts for low-frequency events, like cyanobacterial growth events, is
628 especially challenging and uncertainty partitioning in these highly dynamic systems can help
629 prioritize research to improve process understanding or increase sampling frequency in space or
630 time. Standardized and formal uncertainty partitioning across studies and ecosystems could
631 identify consistent or contrasting patterns in forecast skill at different horizons in ecosystems
632 where low-frequency or rare events have significant consequences, such as cyanobacterial
633 blooms (Kim et al. 2014) and insect (Hobbs et al. 2015) and disease outbreaks (Grünwald et al.
634 2000). Overall, despite considering dozens of possible environmental covariates, our hindcasts
635 were not skilled enough to predict the sudden, infrequent increases in cyanobacterial density that
636 cause concern for water resource managers and other stakeholders in both oligotrophic and
637 eutrophic lakes. However, formal uncertainty partitioning provided insight on how to target data
638 collection and modeling efforts, following Dietze et al. (2018). Even if our initial forecasting
639 efforts are not very skilled, the process of iteratively confronting our models with data and
640 quantitatively examining forecast uncertainty teaches us how to improve (Bauer et al. 2015).
641 Access to data and standardized expectations for uncertainty partitioning are critical to the

642 iterative improvement of forecast skill. Our study was enabled both by collaborative sharing of
643 long-term data through the Global Lake Ecological Observatory Network, which facilitated
644 calibration and validation of hindcasting models over many years (Cottingham et al. 2020a,
645 2020b, LSPA et al. 2020a, 2020b), and access to publicly available R code examples of how to
646 conduct uncertainty partitioning (https://github.com/EcoForecast/EF_Activities). As such, our
647 study illustrates the importance of open science and findable, accessible, interoperable, and
648 reusable (FAIR) scientific practices with respect to data and code (Wilkinson et al. 2016, Powers
649 and Hampton 2019) to reduce barriers to adoption of techniques such as uncertainty partitioning
650 and advance the field of ecological forecasting.

651

652

653 **Acknowledgments**

654 The study was initiated as part of a Global Lake Ecological Observatory Network Fellowship
655 Program Bayesian statistics workshop. MEL led development of Bayesian state-space models
656 with SLL and conducted hindcasts and variance partitioning, with substantial contributions from
657 JAB, WSB, JAZ, and MCD. KLC, HAE, KCW, and CCC contributed data. BGS led publication
658 of datasets. All authors provided feedback on the design and scope of the modeling effort, the
659 interpretation of results, and edited and approved the final version of the manuscript. The long-
660 term Sunapee data collection was funded by NSF (DBI-0434684, DEB-0749022, EF-0842267,
661 EF-0842112, EF-0842125, DEB-1010862, CNS-1737424, ICER-1517823), Lake Sunapee
662 Protective Association, Dartmouth College, Auburn Water District/Lewiston Water Division,
663 and Bates College. The forecasting project was funded by NSF MSB DEB-1638575, DEB-
664 1137327, DEB-1702991, and DEB-1638577. MEL and CCC were supported by NSF CNS-

665 1737424, DEB-1753639, DBI-1933016, and MSB DEB-1926050. MEL was supported by a
666 Virginia Water Resources Research Center William R. Walker Graduate Research Fellow Award
667 and a Virginia Tech College of Science Make-A-Difference Roundtable Scholarship. JAB was
668 supported by funding from the Ecology, Evolution, Environment, and Society program at
669 Dartmouth College and a Midge Eliassen Fellowship. The Eliassen and Fichter families provided
670 generous access to study sites. Special thanks to all of the participants in the December 2017
671 Global Lake Ecological Observatory Network (GLEON) Bayesian statistics workshop for idea
672 development, to John Foster and other participants in the January 2019 Near-term Ecological
673 Forecasting Initiative workshop for assistance with model development, and to the Spring 2020
674 Ecological Forecasting seminar class at Virginia Tech for help with literature review, as well as
675 to Hilary Dugan and Nicole Ward for help downloading and processing NLDAS data. GLEON
676 and Ecological Forecasting Initiative (EFI) colleagues provided helpful comments.

677

678

679 **Literature Cited**

- 680 Barbiero, R. P., and E. B. Welch. 1992. Contribution of benthic blue-green algal recruitment to
681 lake populations and phosphorus translocation. *Freshwater Biology* 27:249–260.
- 682 Bauer, P., A. Thorpe, and G. Brunet. 2015. The quiet revolution of numerical weather prediction.
683 *Nature* 525:47–55.
- 684 Bormans, M., P. W. Ford, and L. Fabbro. 2005. Spatial and temporal variability in
685 cyanobacterial populations controlled by physical processes. *Journal of Plankton Research*
686 27:61–70.

687

688 Carey, C. C., H. A. Ewing, K. L. Cottingham, K. C. Weathers, R. Q. Thomas, and J. F. Haney.
689 2012a. Occurrence and toxicity of the cyanobacterium *Gloeotrichia echinulata* in low-
690 nutrient lakes in the northeastern United States. *Aquatic Ecology* 46:395–409.

691 Carey, C. C., B. W. Ibelings, E. P. Hoffmann, D. P. Hamilton, and J. D. Brookes. 2012b. Eco-
692 physiological adaptations that favour freshwater cyanobacteria in a changing climate. *Water*
693 *Research* 46:1394–1407.

694 Carey, C. C., K. C. Weathers, and K. L. Cottingham. 2008. *Gloeotrichia echinulata* blooms in an
695 oligotrophic lake: Helpful insights from eutrophic lakes. *Journal of Plankton Research*
696 30:893–904.

697 Carey, C. C., K. C. Weathers, H. A. Ewing, M. L. Greer, and K. L. Cottingham. 2014. Spatial
698 and temporal variability in recruitment of the cyanobacterium *Gloeotrichia echinulata* in an
699 oligotrophic lake. *Freshwater Science* 33:577–592.

700 Carlson, R. E. 1977. A trophic state index for lakes. *Limnology and Oceanography* 22:361–369.

701 Carlson, R., and J. Simpson. 1996. *A Coordinator's Guide to Volunteer Lake Monitoring*
702 *Methods*. North American Lake Management Society.

703 Carpenter, S. R., B. M. S. Arani, P. C. Hanson, M. Scheffer, E. H. Stanley, and E. Van Nes.
704 2020. Stochastic dynamics of Cyanobacteria in long-term high-frequency observations of a
705 eutrophic lake. *Limnology and Oceanography Letters*.

706 Catherine, A., N. Escoffier, A. Belhocine, A. B. Nasri, S. Hamlaoui, C. Yéprémian, C. Bernard,
707 and M. Troussellier. 2012. On the use of the FluoroProbe®, a phytoplankton quantification
708 method based on fluorescence excitation spectra for large-scale surveys of lakes and
709 reservoirs. *Water Research* 46:1771–1784.

710 Clark, J. 2007. *Models for ecological data*. Princeton University Press, Princeton, NJ, USA.

711 Clark, J. S., S. R. Carpenter, M. Barber, S. Collins, A. Dobson, J. A. Foley, D. M. Lodge, M.
712 Pascual, J. Pielke R., W. Pizer, C. Pringle, W. V. Reid, K. A. Rose, O. Sala, W. H.
713 Schlesinger, D. H. Wall, and D. Wear. 2001. Ecological forecasts: An emerging imperative.
714 Science 293:657–660.

715 Cobourn, K. M., C. C. Carey, K. J. Boyle, C. Duffy, H. A. Dugan, K. J. Farrell, L. Fitchett, P. C.
716 Hanson, J. A. Hart, V. R. Henson, A. L. Hetherington, A. R. Kemanian, L. G. Rudstam, L.
717 Shu, P. A. Soranno, M. G. Sorice, J. Stachelek, N. K. Ward, K. C. Weathers, W. Weng, and
718 Y. Zhang. 2018. From concept to practice to policy: modeling coupled natural and human
719 systems in lake catchments. Ecosphere 9:1–15.

720 Cottingham, K. L. 2020. Surface pelagic total nitrogen concentrations in Lake Sunapee, USA
721 2009 to 2012. Environmental Data Initiative.

722 Cottingham, K. L., C. C. Carey, and K. C. Weathers. 2020a. *Gloeotrichia echinulata* density at
723 four nearshore sites in Lake Sunapee, NH, USA from 2005-2016 ver. 2. Environmental
724 Data Initiative.

725 Cottingham, K. L., C. C. Carey, and K. C. Weathers. 2020b. High-frequency temperature data
726 from four near-shore sites, Lake Sunapee, NH, USA, 2006-2018. Environmental Data
727 Initiative.

728 Cottingham, K. L., H. A. Ewing, M. L. Greer, C. C. Carey, and K. C. Weathers. 2015.
729 Cyanobacteria as biological drivers of lake nitrogen and phosphorus cycling. Ecosphere
730 6:1–19.

731 Cyr, H. 2017. Winds and the distribution of nearshore phytoplankton in a stratified lake. Water
732 Research 122:114–127.

733

734 Denwood, M., and M. Plummer. 2019. Interface Utilities, Model Templates, Parallel Computing
735 Methods and Additional Distributions for MCMC Models in JAGS v. 2.0.4-2.

736 Dietze, M. C. 2017a. Ecological Forecasting. 1st edition. Princeton University Press, Princeton,
737 NJ, USA.

738 Dietze, M. C. 2017b. Prediction in ecology: A first-principles framework: A. Ecological
739 Applications 27:2048–2060.

740 Dietze, M. C., A. Fox, L. M. Beck-Johnson, J. L. Betancourt, M. B. Hooten, C. S. Jarnevich, T.
741 H. Keitt, M. A. Kenney, C. M. Laney, L. G. Larsen, H. W. Loescher, C. K. Lunch, B. C.
742 Pijanowski, J. T. Randerson, E. K. Read, A. T. Tredennick, R. Vargas, K. C. Weathers, and
743 E. P. White. 2018. Iterative near-term ecological forecasting: Needs, opportunities, and
744 challenges. Proceedings of the National Academy of Sciences of the United States of
745 America 115:1424–1432.

746 Diniz-Filho, A. F., L. M. Bini, T. F. Rangel, R. D. Loyola, C. Hof, D. Nogue, and M. B. Arau.
747 2009. Partitioning and mapping uncertainties in ensembles of forecasts of species turnover
748 under climate change. Ecography 32:897–906.

749 Dodds, W., W. W. Bouska, J. L. Eitzmann, T. J. Pilger, K. L. Pitts, A. J. Riley, J. T. Schloesser,
750 and D. J. Thornbrugh. 2009. Eutrophication of U.S. Freshwaters: Analysis of Potential
751 Economic Damages. Environmental Science & Technology 43:12–19.

752 Dokulil, M. T., and K. Teubner. 2000. Cyanobacterial Dominance in Lakes. Hydrobiologia
753 438:1–12.

754 van Dolah, E. R., M. Paolisso, K. Sellner, and A. Place. 2015. Employing a socio-ecological
755 systems approach to engage harmful algal bloom stakeholders. Aquatic Ecology 50:1–18.
756

757 de Eyto, E., E. Jennings, E. Ryder, K. Sparber, M. Dillane, C. Dalton, and R. Poole. 2016.
758 Response of a humic lake ecosystem to an extreme precipitation event: physical, chemical,
759 and biological implications. *Inland Waters*:483–498.

760 Fox, A. M., T. J. Hoar, J. L. Anderson, A. F. Arellano, W. K. Smith, M. E. Litvak, N. MacBean,
761 D. S. Schimel, and D. J. P. Moore. 2018. Evaluation of a Data Assimilation System for
762 Land Surface Models Using CLM4.5. *Journal of Advances in Modeling Earth Systems*
763 10:2471–2494.

764 Franks, P. J. S. 1997. Spatial patterns in dense algal blooms. *Limnology and Oceanography*
765 42:1297–1305.

766 Freeman, E. C., I. F. Creed, B. Jones, and A.-K. Bergstrom. 2020. Global changes may be
767 promoting a rise in select cyanobacteria in nutrient-poor northern lakes. *Global Change*
768 *Biology*.

769 Gelfand, A. E., and S. K. Ghosh. 1998. Model Choice : A Minimum Posterior Predictive Loss
770 Approach. *Biometrika Trust* 85:1–11.

771 Gertner, G., P. Parysow, and B. Guan. 1996. Projection Variance Partitioning of a Conceptual
772 Forest Growth Model with Orthogonal Polynomials. *Forest Science* 42:474–486.

773 Gibson, G., R. Carlson, J. Simpson, E. Smeltzer, J. Gerritson, S. Chapra, S. Heiskary, J. Jones,
774 and R. Kennedy. 2000. USEPA Nutrient Criteria Technical Guidance Manual Lakes and
775 Reservoirs. United States Environmental Protection Agency.

776 Grünwald, N. J., O. A. Rubio-Covarrubias, and W. E. Fry. 2000. Potato late-blight management
777 in the Toluca Valley: Forecasts and resistant cultivars. *Plant Disease* 84:410–416.

778 Hamilton, G., R. McVinish, and K. Mengersen. 2009. Bayesian model averaging for harmful
779 algal bloom prediction. *Ecological Applications* 19:1805–1814.

780 Hobbs, N. T., C. Geremia, J. Treanor, R. Wallen, P. J. White, M. B. Hooten, and J. C. Rhyan.
781 2015. State-space modeling to support management of brucellosis in the Yellowstone bison
782 population. *Ecological Monographs* 85:525–556.

783 Hobbs, N. T., and M. B. Hooten. 2015. *Bayesian Models: A Statistical Primer for Ecologists*. 1st
784 edition. Princeton University Press, Princeton, NJ, USA.

785 Hobday, A. J., J. R. Hartog, J. P. Manderson, K. E. Mills, M. J. Oliver, A. J. Pershing, and S.
786 Siedlecki. 2019. Ethical considerations and unanticipated consequences associated with
787 ecological forecasting for marine resources. *ICES Journal of Marine Science* 76:1244–1256.

788 Huang, J., J. Gao, J. Liu, and Y. Zhang. 2013. State and parameter update of a hydrodynamic-
789 phytoplankton model using ensemble Kalman filter. *Ecological Modelling* 263:81–91.

790 Huisman, J., and F. D. Hulot. 2005. Population Dynamics of Harmful Cyanobacteria. Pages 143–
791 176 in J. Huisman, H. C. P. Matthijs, and P. M. Visser, editors. *Harmful Cyanobacteria*.
792 Aquatic Ecology Series, vol. 3 Springer, Dordrecht.

793 Hyenstrand, P., E. Rydin, and M. Gunnerhed. 2000. Response of pelagic cyanobacteria to iron
794 additions--enclosure experiments from Lake Erken. *Journal of Plankton Research* 22:1113–
795 1126.

796 Ibelings, B. W., M. Bormans, J. Fastner, and P. M. Visser. 2016. CYANOCOST special issue on
797 cyanobacterial blooms: synopsis-a critical review of the management options for their
798 prevention, control and mitigation. *Aquatic Ecology* 50:1–11.

799 Idso, S. B. 1973. On the concept of lake stability. *Limnol. Oceanogr.* 18:681–683.

800 Istvánovics, V., K. Pettersson, M. A. Rodrigo, D. Pierson, J. Padišk, and W. Colom. 1993.
801 *Gloeotrichia echinulata*, a colonial cyanobacterium with a unique phosphorus uptake and
802 life strategy. *Journal of Plankton Research* 15:531–552.

803 Janssen, A. B., J. H. Janse, A. H. Beusen, M. Chang, J. A. Harrison, I. Huttunen, X. Kong, J.
804 Rost, S. Teurlincx, T. A. Troost, D. van Wijk, and W. M. Mooij. 2019. How to model algal
805 blooms in any lake on earth. *Current Opinion in Environmental Sustainability* 36:1–10.

806 Jennings, E., S. Jones, L. Arvola, P. A. Staehr, E. Gaiser, I. D. Jones, K. C. Weathers, G. A.
807 Weyhenmeyer, C. Y. Chiu, and E. De Eyto. 2012. Effects of weather-related episodic
808 events in lakes: an analysis based on high-frequency data. *Freshwater Biology* 57:589–601.

809 Jiang, J., Y. Huang, S. Ma, M. Stacy, Z. Shi, D. M. Ricciuto, P. J. Hanson, and Y. Luo. 2018.
810 Forecasting Responses of a Northern Peatland Carbon Cycle to Elevated CO₂ and a
811 Gradient of Experimental Warming. *Journal of Geophysical Research: Biogeosciences*
812 123:1057–1071.

813 Johansson, M. A., K. M. Apfeldorf, S. Dobson, J. Devita, A. L. Buczak, B. Baugher, L. J. Moniz,
814 T. Bagley, S. M. Babin, E. Guven, T. K. Yamana, J. Shaman, T. Moschou, N. Lothian, A.
815 Lane, G. Osborne, G. Jiang, L. C. Brooks, D. C. Farrow, S. Hyun, R. J. Tibshirani, R.
816 Rosenfeld, J. Lessler, N. G. Reich, D. A. T. Cummings, S. A. Lauer, S. M. Moore, H. E.
817 Clapham, R. Lowe, T. C. Bailey, M. García-Díez, M. S. Carvalho, X. Rodó, T. Sardar, R.
818 Paul, E. L. Ray, K. Sakrejda, A. C. Brown, X. Meng, O. Osoba, R. Vardavas, D. Manheim,
819 M. Moore, D. M. Rao, T. C. Porco, S. Ackley, F. Liu, L. Worden, M. Convertino, Y. Liu,
820 A. Reddy, E. Ortiz, J. Rivero, H. Brito, A. Juarrero, L. R. Johnson, R. B. Gramacy, J. M.
821 Cohen, E. A. Mordecai, C. C. Murdock, J. R. Rohr, S. J. Ryan, A. M. Stewart-Ibarra, D. P.
822 Weikel, A. Jutla, R. Khan, M. Poultney, R. R. Colwell, B. Rivera-García, C. M. Barker, J.
823 E. Bell, M. Biggerstaff, D. Swerdlow, L. Mier-Y-Teran-Romero, B. M. Forshey, J. Trtanj,
824 J. Asher, M. Clay, H. S. Margolis, A. M. Hebbeler, D. George, and J. P. Chretien. 2019. An
825 open challenge to advance probabilistic forecasting for dengue epidemics. *Proceedings of*

826 the National Academy of Sciences of the United States of America 116:24268–24274.

827 Jolliffe, I., and D. Stephenson. 2003. *Forecast Verification : A Practitioner’s Guide in*

828 *Atmospheric Science*. 2nd edition. Wiley, Chichester, West Sussex, England.

829 Karlsson-Elfgren, I., P. Hyenstrand, and E. Riydin. 2005. Pelagic growth and colony division of

830 *Gloeotrichia echinulata* in Lake Erken. *Journal of Plankton Research* 27:145–151.

831 Karlsson-Elfgren, I., K. Rengefors, and S. Gustafsson. 2004. Factors regulating recruitment from

832 the sediment to the water column in the bloom-forming cyanobacterium *Gloeotrichia*

833 *echinulata*. *Freshwater Biology* 49:265–273.

834 Kauffman, G. J. 2016. Economic Value of Nature and Ecosystems in the Delaware River Basin.

835 *Journal of Contemporary Water Research & Education* 158:98–119.

836 Kim, K., M. Park, J. H. Min, I. Ryu, M. R. Kang, and L. J. Park. 2014. Simulation of algal bloom

837 dynamics in a river with the ensemble Kalman filter. *Journal of Hydrology* 519:2810–2821.

838 Kuha, J., L. Arvola, P. Hanson, J. Huotari, T. Huttula, J. Juntunen, M. Jarvinen, K. Kallio, M.

839 Ketola, K. Kuoppamaki, A. Lepisto, A. Lohila, R. Paavola, J. Vuorenmaa, L. Winslow, and

840 J. Karjalainen. 2016. Response of boreal lakes to episodic weather-induced events. *Inland*

841 *Waters* 6:523–534.

842 Kuikka, S., J. Vanhatalo, H. Pulkkinen, S. Mäntyniemi, and J. Corander. 2014. Experience in

843 Bayesian Inference in Baltic Salmon Management. *Statistical Science* 29:42–49.

844 Küpper, H., S. Seibert, and A. Parameswaran. 2007. Fast, sensitive, and inexpensive alternative

845 to analytical pigment HPLC: Quantification of chlorophylls and carotenoids in crude

846 extracts by fitting with Gauss peak spectra. *Analytical Chemistry* 79:7611–7627.

847

848

849 Lofton, M. E., J. A. Brentrup, W. S. Beck, J. A. Zwart, R. Bhattacharya, L. S. Brighenti, S. H.
850 Burnet, I. M. McCullough, B. G. Steele, C. C. Carey, K. L. Cottingham, M. C. Dietze, H. A.
851 Ewing, K. C. Weathers, and S. L. LaDeau. 2020. Lake Sunapee *Gloeotrichia echinulata*
852 density near-term hindcasts from 2015-2016 and meteorological model driver data,
853 including shortwave radiation and precipitation from 2009-2016 ver 4. Environmental Data
854 Initiative staging environment.

855 LSPA; Lake Sunapee Protective Association, K. C. Weathers, and B. G. Steele. 2020. Lake
856 Sunapee Instrumented Buoy: High Frequency Water Temperature and Dissolved Oxygen
857 Data – 2007-2019. Environmental Data Initiative.

858 LSPA; Lake Sunapee Protective Association, B. Steele, and K. C. Weathers. 2020. Lake Sunapee
859 High Frequency Weather Data measured on buoy - 2007-2017 ver. 3. Environmental Data
860 Initiative.

861 Madgwick, G., I. D. Jones, S. J. Thackeray, J. A. Elliott, and H. J. Miller. 2006. Phytoplankton
862 communities and antecedent conditions: high resolution sampling in Esthwaite Water.
863 *Freshwater Biology* 51:1798–1810.

864 Massoud, E. C., J. Huisman, E. Beninca, M. C. Dietze, W. Bouten, and J. A. Vrugt. 2018.
865 Probing the limits of predictability: data assimilation of chaotic dynamics in complex food
866 webs. *Ecology Letters* 21:93–103.

867 Mbogga, M. S., X. Wang, and A. Hamann. 2010. Bioclimate envelope model predictions for
868 natural resource management: dealing with uncertainty. *Journal of Applied Ecology*
869 47:731–740.

870

871

872 McGowan, J. A., E. R. Deyle, H. Ye, M. L. Carter, C. T. Perretti, M. Hilbern, K. Seger, A. de
873 Verniel, and G. Sugihara. 2017. Predicting coastal algal blooms in Southern California
874 98:1419–1433.

875 Mueller, H., D. P. Hamilton, and G. J. Doole. 2016. Evaluating services and damage costs of
876 degradation of a major lake ecosystem. *Ecosystem Services* 22:370–380.

877 Napiórkowska-Krzebietke, A., and A. Hutorowicz. 2015. The physicochemical background for
878 the development of potentially harmful cyanobacterium *Gloeotrichia echinulata* J. S. Smith
879 ex Richt. *Journal of Elementology* 20:363–376.

880 Ndong, M., D. Bird, T. Nguyen Quang, R. Kahawita, D. Hamilton, M. L. de Boutray, M.
881 Prévost, and S. Dorner. 2017. A novel Eulerian approach for modelling cyanobacteria
882 movement: Thin layer formation and recurrent risk to drinking water intakes. *Water*
883 *Research* 127:191–203.

884 O’Neil, J. M., T. W. Davis, M. A. Burford, and C. J. Gobler. 2012. The rise of harmful
885 cyanobacteria blooms: The potential roles of eutrophication and climate change. *Harmful*
886 *Algae* 14:313–334.

887 Ouellet-Proulx, S., O. Chimi Chiadjeu, M. A. Boucher, and A. St-Hilaire. 2017. Assimilation of
888 water temperature and discharge data for ensemble water temperature forecasting. *Journal*
889 *of Hydrology* 554:342–359.

890 Paerl, H. W., N. S. Hall, and E. S. Calandrino. 2011. Controlling harmful cyanobacterial blooms
891 in a world experiencing anthropogenic and climatic-induced change. *Science of the Total*
892 *Environment* 409:1739–1745.

893 Paerl, H. W., and J. Huisman. 2008. Blooms Like It Hot. *Science* 320:57–58.

894

895 Paerl, H. W., and T. G. Otten. 2013. Harmful Cyanobacterial Blooms: Causes, Consequences,
896 and Controls. *Microbial Ecology* 65:995–1010.

897 Page, T., P. J. Smith, K. J. Beven, I. D. Jones, J. A. Elliott, S. C. Maberly, E. B. Mackay, M. De
898 Ville, and H. Feuchtmayr. 2017. Constraining uncertainty and process-representation in an
899 algal community lake model using high frequency in-lake observations. *Ecological*
900 *Modelling* 357:1–13.

901 Page, T., P. J. Smith, K. J. Beven, I. D. Jones, J. A. Elliott, S. C. Maberly, E. B. Mackay, M. De
902 Ville, and H. Feuchtmayr. 2018. Adaptive forecasting of phytoplankton communities.
903 *Water Research* 134:74–85.

904 Plummer, M., A. Stukalov, and M. Denwood. 2019. Bayesian Graphical Models using MCMC.

905 Powers, S. M., and S. E. Hampton. 2019. Open science, reproducibility, and transparency in
906 ecology. *Ecological Applications* 29:1–8.

907 Ravindranath, A., N. Devineni, and P. Kolesar. 2016. An environmental perspective on the water
908 management policies of the Upper Delaware River Basin. *Water Policy* 18:1399–1419.

909 Reynolds, C. S., J. Alex Elliott, and M. A. Frassl. 2014. Predictive utility of trait-separated
910 phytoplankton groups: A robust approach to modeling population dynamics. *Journal of*
911 *Great Lakes Research* 40:143–150.

912 Rigosi, A., W. Fleenor, and F. Rueda. 2010. State-of-the-art and recent progress in
913 phytoplankton succession modelling. *Environmental Reviews* 18:423–440.

914 Roelofs, T. D., and R. T. Oglesby. 1970. Ecological Observations on the Planktonic Cyanophyte
915 *Gleotrichia Echinulata*. *Limnol. Oceanogr.* 15:224–229.

916

917

918 Rolland, D. C., S. Bourget, A. Warren, I. Laurion, and W. F. Vincent. 2013. Extreme variability
919 of cyanobacterial blooms in an urban drinking water supply. *Journal of Plankton Research*
920 35:744–758.

921 Rott, E., N. Salmaso, and E. Hoehn. 2007. Quality control of Utermöhl-based phytoplankton
922 counting and biovolume estimates - An easy task or a Gordian knot? *Hydrobiologia*
923 578:141–146.

924 Rouso, B. Z., E. Bertone, R. Stewart, and D. P. Hamilton. 2020. A systematic literature review
925 of forecasting and predictive models for cyanobacteria blooms in freshwater lakes. *Water*
926 *Research*.

927 Schindler, D. W., and J. R. Vallentyne. 2008. *The algal bowl: overfertilization of the world's*
928 *freshwaters and estuaries*. 1st edition. University of Alberta Press, Edmonton.

929 Serizawa, H., T. Amemiya, and K. Itoh. 2008. Patchiness in a minimal nutrient - phytoplankton
930 model. *Journal of Biosciences* 33:391–403.

931 Shuman, F. G. 1989. History of Numerical Weather Prediction at the National Meteorological
932 Center. *Weather and Forecasting* 4:286–296.

933 Stoddard, J. L., J. Van Sickle, A. T. Herlihy, J. Brahney, S. Paulsen, D. V. Peck, R. Mitchell, and
934 A. I. Pollard. 2016. Continental-Scale Increase in Lake and Stream Phosphorus: Are
935 Oligotrophic Systems Disappearing in the United States? *Environmental Science and*
936 *Technology* 50:3409–3415.

937 Stroom, J. M., and W. E. A. Kardinaal. 2016. How to combat cyanobacterial blooms: strategy
938 toward preventive lake restoration and reactive control measures. *Aquatic Ecology* 50:1–36.

939

940

941 Stumpf, R. P., Mi. C. Tomlinson, J. A. Calkins, B. Kirkpatrick, K. Fisher, K. Nierenberg, R.
942 Currier, and T. T. Wynne. 2009. Skill assessment for an operational algal bloom forecast
943 system. *Journal of Marine Systems* 76:151–161.

944 Thomas, R. Q., R. J. Figueiredo, V. Daneshmand, B. J. Bookout, L. K. Puckett, and C. C. Carey.
945 2020. A near-term iterative forecasting system successfully predicts reservoir
946 hydrodynamics and partitions uncertainty. *bioRxiv*.

947 Thomas, R. Q., A. L. Jersild, E. B. Brooks, V. A. Thomas, and R. H. Wynne. 2018. A mid-
948 century ecological forecast with partitioned uncertainty predicts increases in loblolly pine
949 forest productivity. *Ecological Applications* 28:1503–1519.

950 Thrane, J. E., M. Kyle, M. Striebel, S. Haande, M. Grung, T. Rohrlack, and T. Andersen. 2015.
951 Spectrophotometric analysis of pigments: A critical assessment of a high-throughput
952 method for analysis of algal pigment mixtures by spectral deconvolution. *PLoS ONE* 10:1–
953 24.

954 U.S. EPA. 1991. Guidance manual for compliance with the filtration and disinfection
955 requirements for public water systems using surface water sources. United States
956 Environmental Protection Agency, Washington, D.C.

957 Valle, D., C. L. Staudhammer, W. P. Cropper, and P. R. Van Gardingen. 2009. The importance
958 of multimodel projections to assess uncertainty in projections from simulation models.
959 *Ecological Applications* 19:1680–1692.

960 Le Vu, B., B. Vinçon-Leite, B. J. Lemaire, N. Bensoussan, M. Calzas, C. Drezen, J. F.
961 Deroubaix, N. Escoffier, Y. Dégrés, C. Freissinet, A. Groleau, J. F. Humbert, G. Paolini, F.
962 Prévoit, C. Quiblier, E. Rioust, and B. Tassin. 2011. High-frequency monitoring of
963 phytoplankton dynamics within the European water framework directive: Application to

964 metalimnetic cyanobacteria. *Biogeochemistry* 106:229–242.

965 Vuorio, K., L. Lepistö, and A. L. Holopainen. 2007. Intercalibrations of freshwater
966 phytoplankton analyses. *Boreal Environment Research* 12:561–569.

967 Wallace, B. B., M. C. Bailey, and D. P. Hamilton. 2000. Simulation of vertical position of
968 buoyancy regulating *Microcystis aeruginosa* in a shallow eutrophic lake. *Aquatic Sciences*
969 62:320–333.

970 Wang, G., T. Oyana, M. Zhang, S. Adu-prah, S. Zeng, H. Lin, and J. Se. 2009. Mapping and
971 spatial uncertainty analysis of forest vegetation carbon by combining national forest
972 inventory data and satellite images. *Forest Ecology and Management* 258:1275–1283.

973 Watling, J. I., L. A. Brandt, D. N. Bucklin, I. Fujisaki, F. J. Mazzotti, S. S. Roma, and C.
974 Speroterra. 2015. Performance metrics and variance partitioning reveal sources of
975 uncertainty in species distribution models. *Ecological Modelling* 309–310:48–59.

976 Wilkinson, M. D., M. Dumontier, I. J. Aalbersberg, G. Appleton, M. Axton, A. Baak, N.
977 Blomberg, J.-W. Boiten, L. B. da Silva Santos, P. E. Bourne, J. Bouwman, A. J. Brookes, T.
978 Clark, M. Crosas, I. Dillo, O. Dumon, S. Edmunds, C. T. Evelo, R. Finkers, A. Gonzalez-
979 Beltran, A. J. G. Gray, P. Groth, C. Goble, J. S. Grethe, J. Heringa, P. A. 't Hoen, R.
980 Hooft, T. Kuhn, R. Kok, J. Kok, S. J. Lusher, M. E. Martone, A. Mons, A. L. Packer, B.
981 Persson, P. Rocca-Serra, M. Roos, R. van Schaik, S.-A. Sansone, E. Schultes, T. Sengstag,
982 T. Slater, G. Strawn, M. a. Swertz, M. Thompson, J. van der Lei, E. van Mulligen, J.
983 Velterop, A. Waagmeester, P. Wittenburg, K. Wolstencroft, J. Zhao, and B. Mons. 2016.
984 The FAIR Guiding Principles for scientific data management and stewardship. *Scientific*
985 *Data* 3:160018.

986

987 Wilson, M. A., and S. R. Carpenter. 1999. Economic valuation of freshwater ecosystem services
988 in the United States: 1971-1997. *Ecological Applications* 9:772–783.

989 Winter, J. G., A. M. Desellas, R. Fletcher, L. Heintsch, A. Morley, L. Nakamoto, and K. Utsumi.
990 2011. Algal blooms in Ontario, Canada: Increases in reports since 1994. *Lake and Reservoir*
991 *Management* 27:107–114.

992 Wynne, T. T., and R. P. Stumpf. 2015. Spatial and temporal patterns in the seasonal distribution
993 of toxic cyanobacteria in western Lake Erie from 2002–2014. *Toxins* 7:1649–1663.

994

995

996

997

998

999

1000

1001 **Tables**

1002 **Table 1:** Terms associated with partitioning uncertainty in ecological models and forecasts. Definitions are adapted from Dietze
 1003 (2017a) unless otherwise specified.

Term	Definition	Example
Credible interval	Interval within which a parameter or model prediction falls with a specified probability; does not include observation uncertainty	95% interval of possible latent values of chlorophyll- <i>a</i> forecasted for tomorrow, incorporating initial conditions, process, parameter, and driver data uncertainty
Driver data uncertainty	Uncertainty arising from observation uncertainty in the estimate or measurement of driver data (environmental predictors of the forecasted state)	Uncertainty in observations of soil temperature needed to drive a soil respiration model; uncertainty in weather forecasts
Hindcast	Predictions of a past time period with specified uncertainty using data (withheld from model calibration) that are iteratively assimilated into the model (Jolliffe and Stephenson 2003)	Making model predictions for tick abundances observed two years ago using a model calibrated to observations from ten years prior.
Initial conditions uncertainty	Uncertainty associated with the starting conditions of a forecasting model run	Uncertainty in initial focal states, such as fish abundance, chlorophyll- <i>a</i> , or soil carbon stock
Observation uncertainty	Difference between the observed data and the true (latent) state that the model is designed to predict; does not propagate forward, so it does not affect the credible interval.	Calibration uncertainty in a temperature sensor; sampling uncertainty when estimating species abundance
Parameter uncertainty	Variance around the model parameter estimates	Uncertainty in the growth rate parameter in a timber yield model
Predictive interval	Interval within which predicted observations are expected to fall with a specified probability; includes observation uncertainty; should be used when comparing models to observed data	95% interval of possible observations of chlorophyll- <i>a</i> forecasted for tomorrow
Process uncertainty	Uncertainty due to model specification (ecological processes that are simplified, absent, or incorrectly represented by the model) or inherent stochasticity in the system	Uncertainty arising from not including an important life history stage in a population growth model; uncertainty arising from demographic stochasticity in plankton communities
Random effects uncertainty	Uncertainty associated with estimation of random effects, which are used to describe shared variance across groups in space and time	Uncertainty in the value of a random site effect in a metacommunity model including many different sampling sites

1004

1005 **Table 2:** List of Bayesian state-space models and covariates. m_t is the latent state of *G. echinulata* density at time t , $N()$ represents a
1006 normal distribution with mean and precision (τ_{proc}). x , $x1$ and $x2$ are environmental covariates in single-covariate and two-covariate
1007 models. β represents parameters for the process model equations.

Model name	Model description	Process model	Covariates
RW	Random walk	$m_{t+1} = N(m_t, \tau_{proc})$	
AR	Autoregressive with one lag (AR(1))	$m_{t+1} = N((\beta_0 + \beta_1 * m_t), \tau_{proc})$	
MinWaterTemp	AR(1) with a single linear covariate	$m_{t+1} = N((\beta_0 + \beta_1 * m_t + \beta_2 * x_{t+1}), \tau_{proc})$	minimum water temperature on sampling day
MinWaterTempLag	AR(1) with a single linear covariate	$m_{t+1} = N((\beta_0 + \beta_1 * m_t + \beta_2 * x_t), \tau_{proc})$	minimum water temperature 1 week prior to the sampling day
WaterTempMA	AR(1) with a single linear covariate	$m_{t+1} = N((\beta_0 + \beta_1 * m_t + \beta_2 * x_t), \tau_{proc})$	seven-day moving average of water temperature including the sampling day
Δ Schmidt	AR(1) with a single linear covariate	$m_{t+1} = N((\beta_0 + \beta_1 * m_t + \beta_2 * (x_{t+1} - x_t)), \tau_{proc})$	difference in median Schmidt stability between 1 week prior to the sampling day and the sampling day
SchmidtLag	AR(1) with a single linear covariate	$m_{t+1} = N((\beta_0 + \beta_1 * m_t + \beta_2 * x_t), \tau_{proc})$	maximum Schmidt stability 1 week prior to the sampling day
WindDir	AR(1) with a single linear covariate	$m_{t+1} = N((\beta_0 + \beta_1 * m_t + \beta_2 * x_t), \tau_{proc})$	proportion of daily wind measurements blowing towards Site 1 with a two-day lag
Precip	AR(1) with a single linear covariate	$m_{t+1} = N((\beta_0 + \beta_1 * m_t + \beta_2 * x_t), \tau_{proc})$	sum of daily precipitation on the sampling day
GDD	AR(1) with a single quadratic covariate	$m_{t+1} = N((\beta_0 + \beta_1 * m_t + \beta_2 * x_t + \beta_3 * x_t^2), \tau_{proc})$	growing degree days
Schmidt+Temp	AR(1) with two linear covariates	$m_{t+1} = N((\beta_0 + \beta_1 * m_t + \beta_2 * x1_t + \beta_3 * x2_t), \tau_{proc})$	difference in median Schmidt stability between 1 week prior the sampling day and the sampling day and seven-day moving average of water temperature including the sampling day
Schmidt+Precip	AR(1) with two linear covariates	$m_{t+1} = N((\beta_0 + \beta_1 * m_t + \beta_2 * x1_t + \beta_3 * x2_t), \tau_{proc})$	difference in median Schmidt stability between the previous sampling day and the day of sampling and sum of daily precipitation on the sampling day
Temp+Precip	AR(1) with two linear covariates	$m_{t+1} = N((\beta_0 + \beta_1 * m_t + \beta_2 * x1_t + \beta_3 * x2_t), \tau_{proc})$	seven-day moving average of water temperature including the sampling day and sum of daily precipitation on the sampling day
Precip+GDD	AR(1) with one linear and one quadratic covariate	$m_{t+1} = N((\beta_0 + \beta_1 * m_t + \beta_2 * x1_t + \beta_3 * x2_t + \beta_4 * x2_t^2), \tau_{proc})$	sum of daily precipitation on the sampling day and growing degree days

1008

1009 **Table 3:** Hindcasting results across models for the 2015-2016 hindcasting period. RMSE = root mean square error; Predictive variance =
1010 mean variance of the predictive interval; Predictive loss = $\sqrt{RMSE^2 + predictive\ variance}$; Δ Predictive loss = the difference between
1011 predictive loss for each model and the best-performing model for that forecast horizon; Coverage = the percent of observations falling
1012 within the 95% predictive interval; Peak timing = the number of weeks between peak *G. echinulata* density during the hindcasting period
1013 and when the model predicted peak density; Bias = mean difference between median predicted and observed values. Note that all
1014 assessment metrics are conducted on log-transformed data except for mean bias. *best-performing models at either the one-week or four-
1015 week forecast horizon based on evaluation of Δ Predictive loss.
1016

Model name	RMSE <i>natural log colonies L⁻¹</i>		Predictive S.D. <i>natural log colonies L²</i>		Predictive loss <i>natural log colonies L²</i>		Δ Predictive loss (Δ PL) <i>natural log colonies L²</i>		Coverage %		Peak timing weeks		Bias <i>colonies L⁻¹</i>	
	1 wk	4 wk	1 wk	4 wk	1 wk	4 wk	1 wk	4 wk	1 wk	4 wk	1 wk	4 wk	1 wk	4 wk
RW	1.89	2.23	1.63	2.98	2.5	3.72	0.25	1.3	97.2	100	1	14	-0.41	-0.96
AR*	1.67	1.61	1.51	2.08	2.25	2.63	0	0.21	97.2	100	1	14	-0.92	-1.52
MinWaterTemp	1.82	1.59	1.43	1.83	2.31	2.43	0.06	0.01	94.4	93.5	14	12	-0.93	-1.41
MinWaterTempLag*	1.79	1.62	1.45	1.79	2.3	2.42	0.05	0	91.7	87.1	14	12	-1	-1.45
WaterTempMA*	1.78	1.59	1.45	1.83	2.3	2.42	0.05	0	94.4	93.5	14	12	-0.95	-1.42
Δ Schmidt*	1.66	1.62	1.52	2.08	2.25	2.63	0	0.21	94.4	100	1	14	-0.91	-1.52
SchmidtLag	1.75	1.58	1.46	2.04	2.28	2.58	0.03	0.16	97.2	100	14	14	-0.9	-1.41
WindDir	1.78	1.55	1.5	2	2.33	2.53	0.08	0.11	94.4	100	1	14	-0.96	-1.51
Precip*	1.66	1.62	1.52	2.09	2.25	2.64	0	0.22	94.4	100	1	14	-0.92	-1.51
GDD	1.84	1.59	1.43	1.84	2.33	2.43	0.08	0.01	94.4	96.8	14	12	-1.08	-1.41
Schmidt+Temp*	1.79	1.61	1.46	1.81	2.31	2.42	0.06	0	91.7	87.1	14	14	-0.97	-1.44
Schmidt+Precip	1.66	1.62	1.53	2.08	2.26	2.64	0.01	0.22	97.2	100	1	14	-0.92	-1.52
Temp+Precip	1.78	1.61	1.46	1.83	2.3	2.43	0.05	0.01	94.4	93.5	14	12	-0.96	-1.43
Precip+GDD	1.81	1.59	1.44	1.84	2.31	2.43	0.06	0.01	97.2	96.8	14	14	-0.88	-1.31
Ensemble	1.76	1.55	1.49	1.97	2.3	2.51	0.05	0.09	97.2	100	14	14	-0.96	-1.48

1017

1018

1019 **Figure legends**

1020 **Figure 1:** Conceptual figure of a Bayesian state-space model, where y_t is the observed
1021 cyanobacterial density at time t , x_t are driver data (environmental covariates) at time t , m_t is the
1022 estimated true, or latent, cyanobacterial density at time t , β is a vector of parameters in the
1023 process model (slope, intercept, etc.), and τ_{proc} and τ_{obs} are the precisions of normal distributions
1024 representing process error and observation error, respectively. Parameters (rounded-edge
1025 rectangle) are modeled as distributions in the parameter model. Parameters, along with driver
1026 data, determine the predicted latent states (ovals; also modeled as a distributions) in the process
1027 model, which are fitted to observations using the data model.

1028 **Figure 2:** Map of Lake Sunapee, New Hampshire, USA with locator map (inset). Data from Site
1029 1 were used for Bayesian state-space models, data from Site 2 were used to inform priors for Site
1030 1 models, and data from Site 3 provided lake-level covariates for Site 1 models.

1031 **Figure 3:** Model development workflow diagram. Model equations and descriptions of
1032 covariates included in each model can be found in Table 2.

1033 **Figure 4:** Timeseries of *G. echinulata* density at Site 1 in Lake Sunapee from 2009-2016 (a, c);
1034 panels b) and d) show a reduced scale to better illustrate variability at low density.

1035 **Figure 5:** Timeseries of median predicted and observed *G. echinulata* density for one-week-
1036 ahead hindcasts in 2015 for the best-performing models (b-g; Table 3), as well as the RW null
1037 model (a). Similar figures for 2016 hindcasts and models not shown here may be in found in the
1038 supplemental material (Fig. S10, S11).

1039 **Figure 6:** Timeseries of median predicted and observed *G. echinulata* density for four-week-
1040 ahead hindcasts in 2015 for the best-performing models (b-g; Table 3), as well as the RW null
1041 model (a). Similar figures for 2016 hindcasts and models not shown here may be in found in the

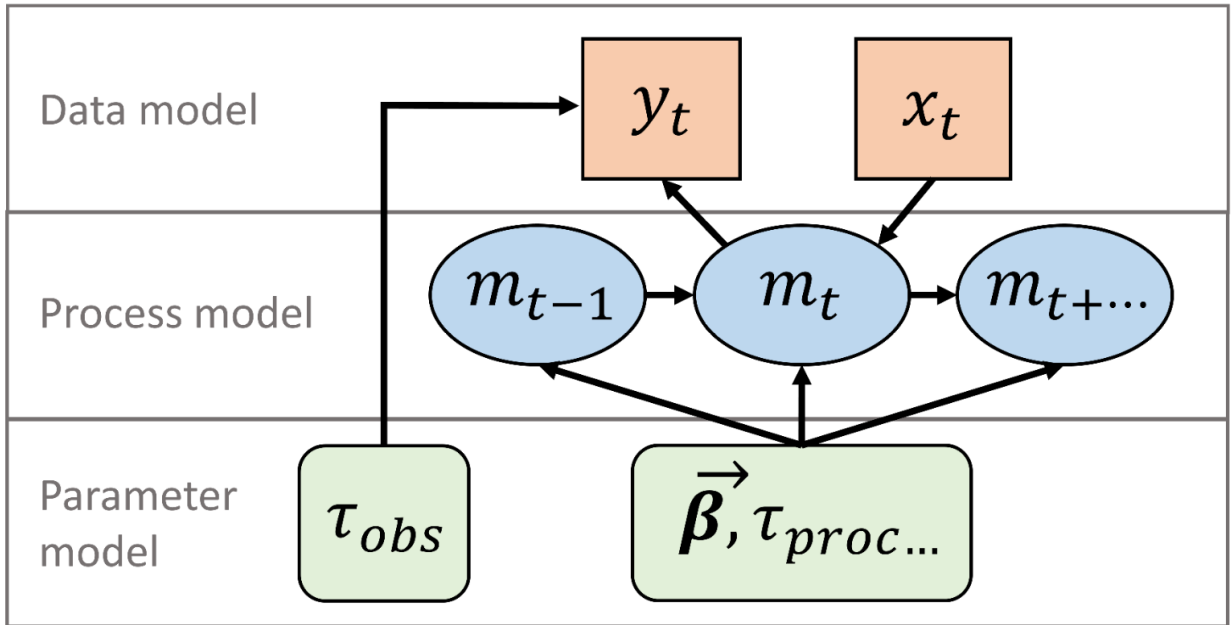
1042 supplemental material (Fig. S12, S13). Note the y-axis change between Figures 5 and 6 to
1043 accommodate larger credible and predictive intervals at the four-week forecast horizon.

1044 **Figure 7:** Uncertainty partitioning of the one-week-ahead to four-week-ahead credible interval
1045 for hindcasts averaged across the 2015-2016 hindcasting period for the best-performing models
1046 (b-g; Table 3), as well as the RW null model (a). Similar figures for other models may be found
1047 in the supplemental material (Fig. S14).

1048 **Figure 8:** Uncertainty partitioning for a) one-week-ahead and b) four-week-ahead hindcasts
1049 averaged across the 2015-2016 hindcasting period across models. White triangles indicate a best-
1050 performing model at the respective forecast horizon as assessed by Δ Predictive loss (Table 3).

1051 **Figures**

1052 **Figure 1**



1053

1054

1055

1056

1057

1058

1059

1060

1061

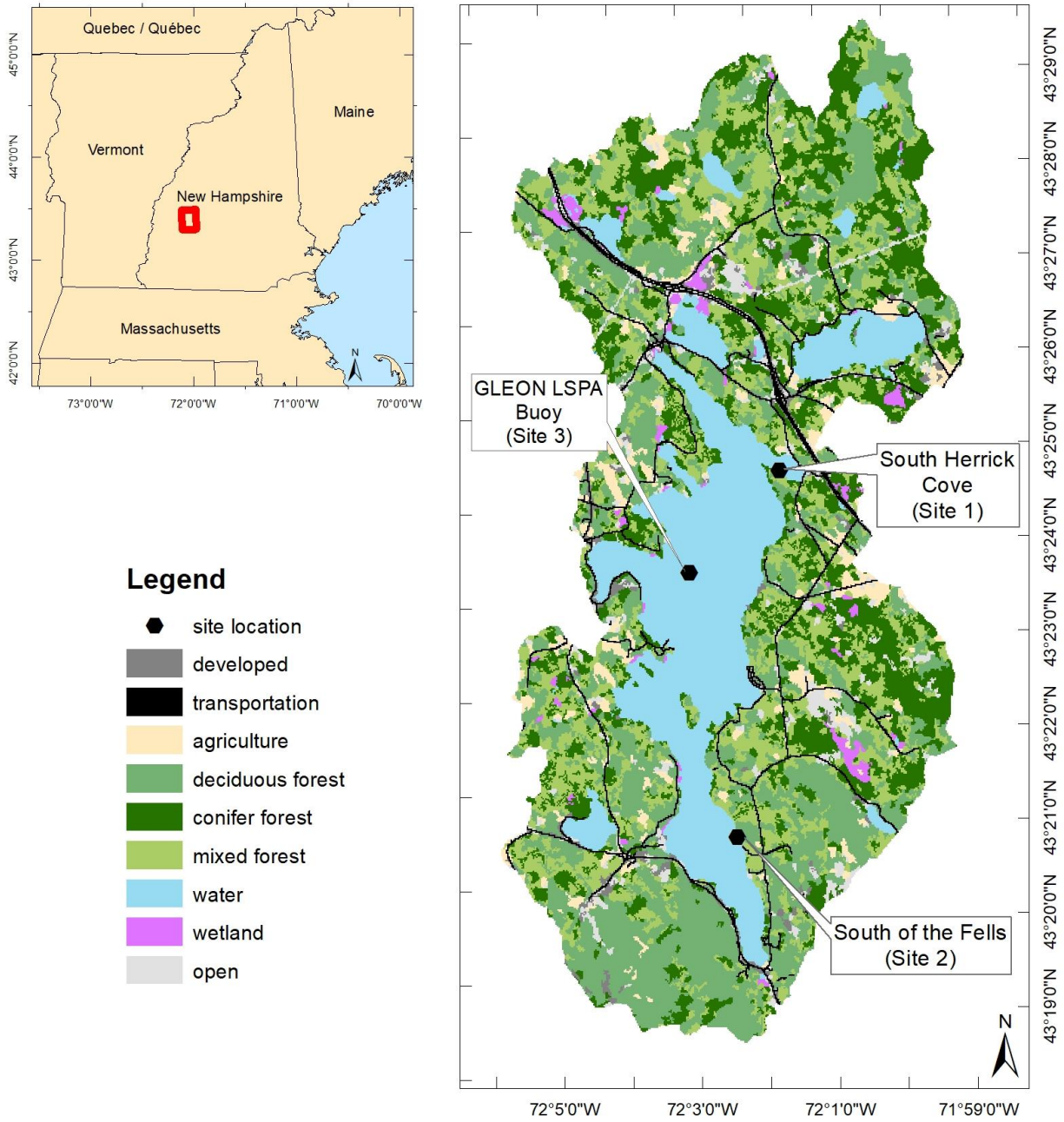
1062

1063

1064

1065

1066 **Figure 2**



1067

1068

1069

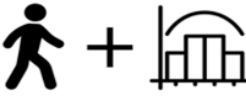
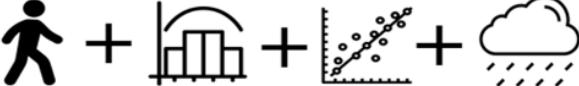
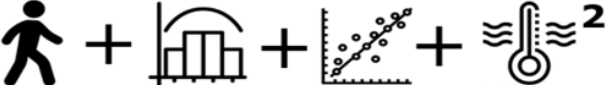
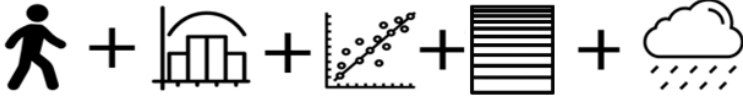
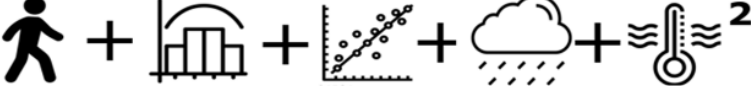
1070

1071

1072 **Figure 3**

Model development workflow

Model names

 <p>Develop random walk null model Add informed observation error prior</p>	<p>RW</p>
 <p>Add linear AR(1) process model</p>	<p>AR</p>
 <p>Add an environmental covariate</p>	<p>MinWaterTemp MinWaterTempLag WaterTempMA ΔSchmidt</p> <p>SchmidtLag WindDir Precip</p>
 <p>Add a quadratic term for environmental covariates if needed Calibrate models using 2009-2014 observed data Validate models using 2015-2016 hindcasts</p>	<p>GDD</p>
 <p>Based on single covariate validation results, add second linear covariate</p>	<p>Schmidt+Temp Schmidt+Precip Temp+Precip</p>
 <p>Add quadratic term to two-covariate models if needed Calibrate and validate all two-covariate models</p>	<p>Precip+GDD</p>

1073

1074

1075

1076

1077

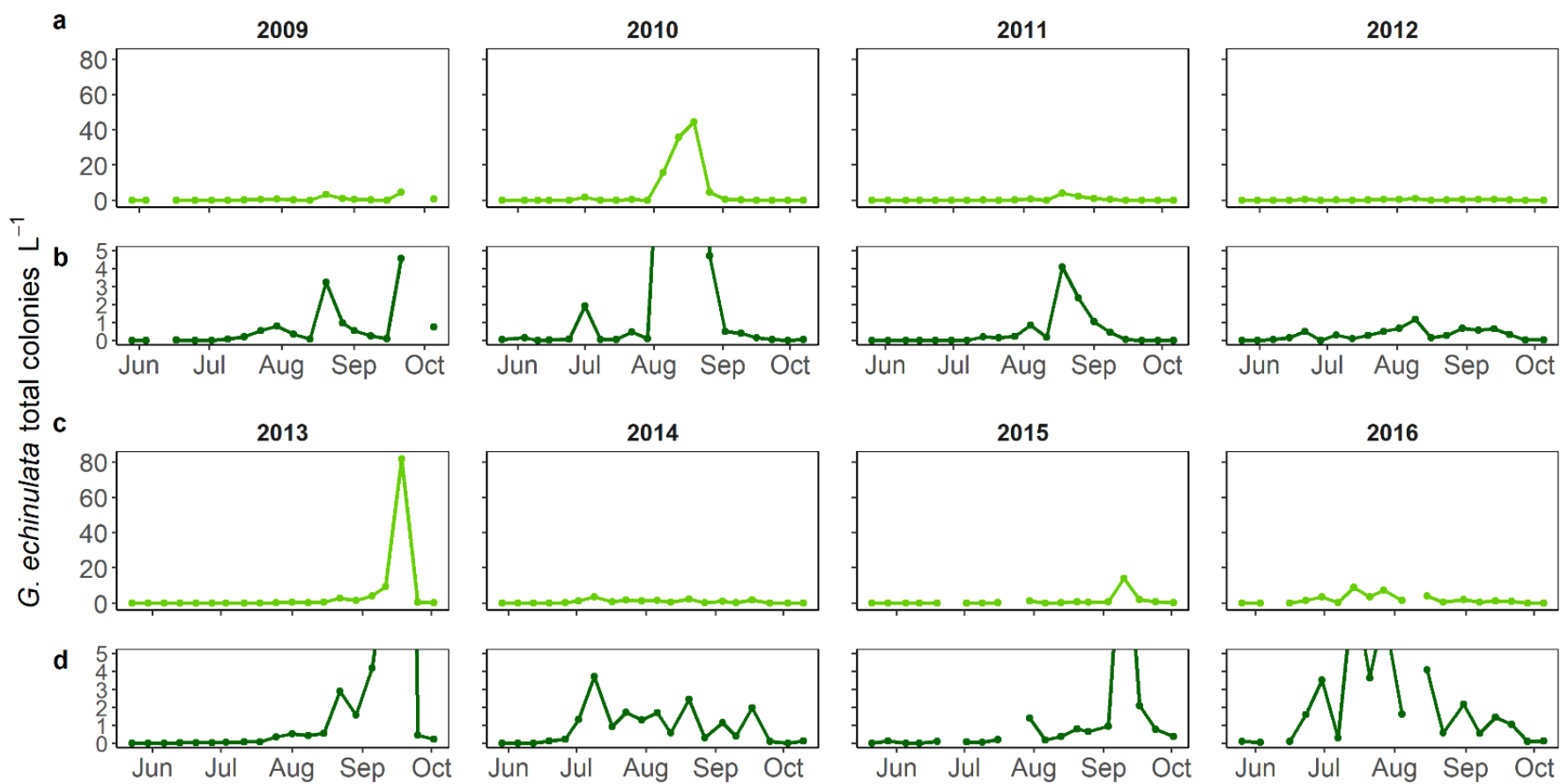
1078

1079

1080

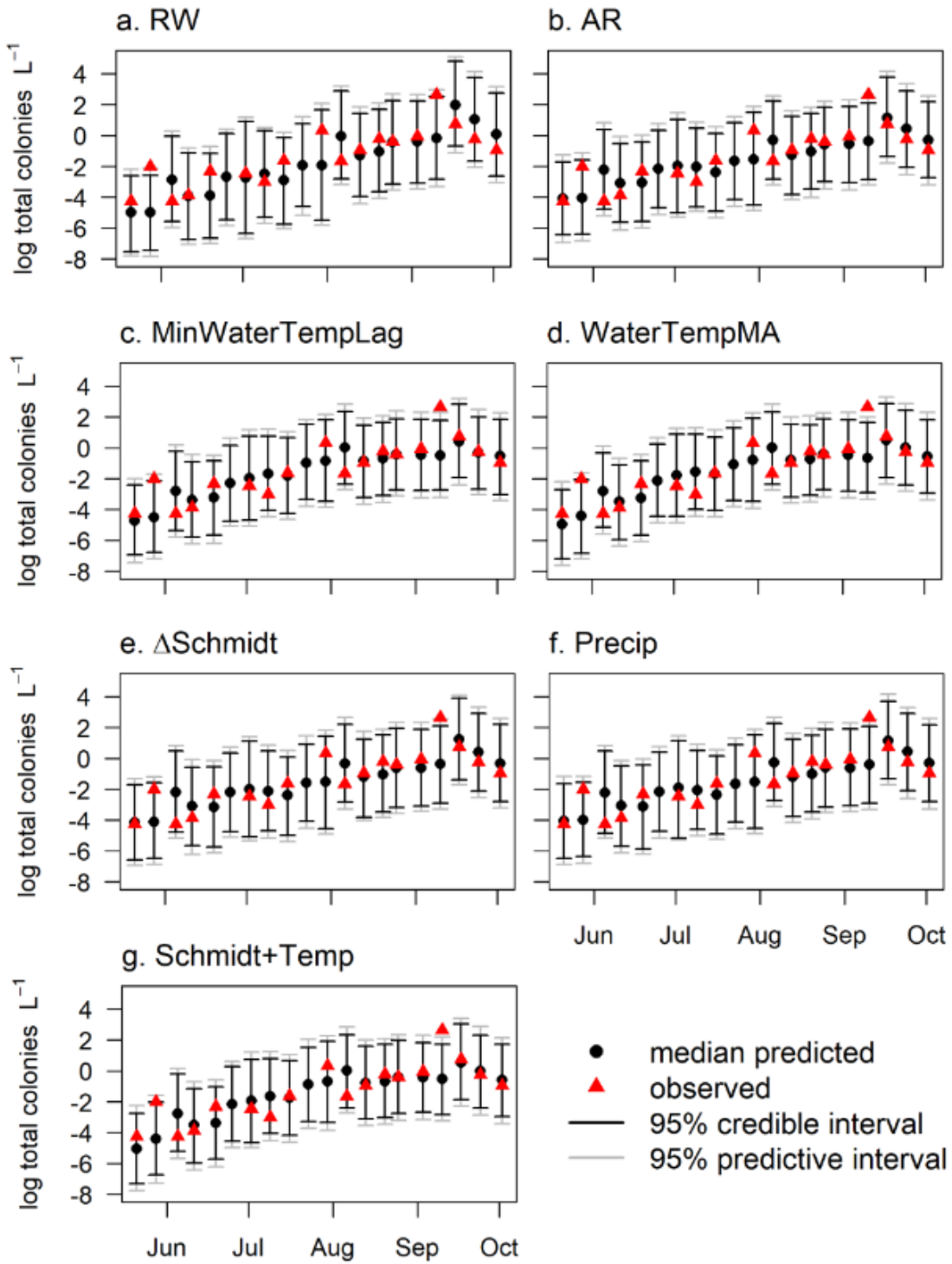
1081

1082 **Figure 4**



1083

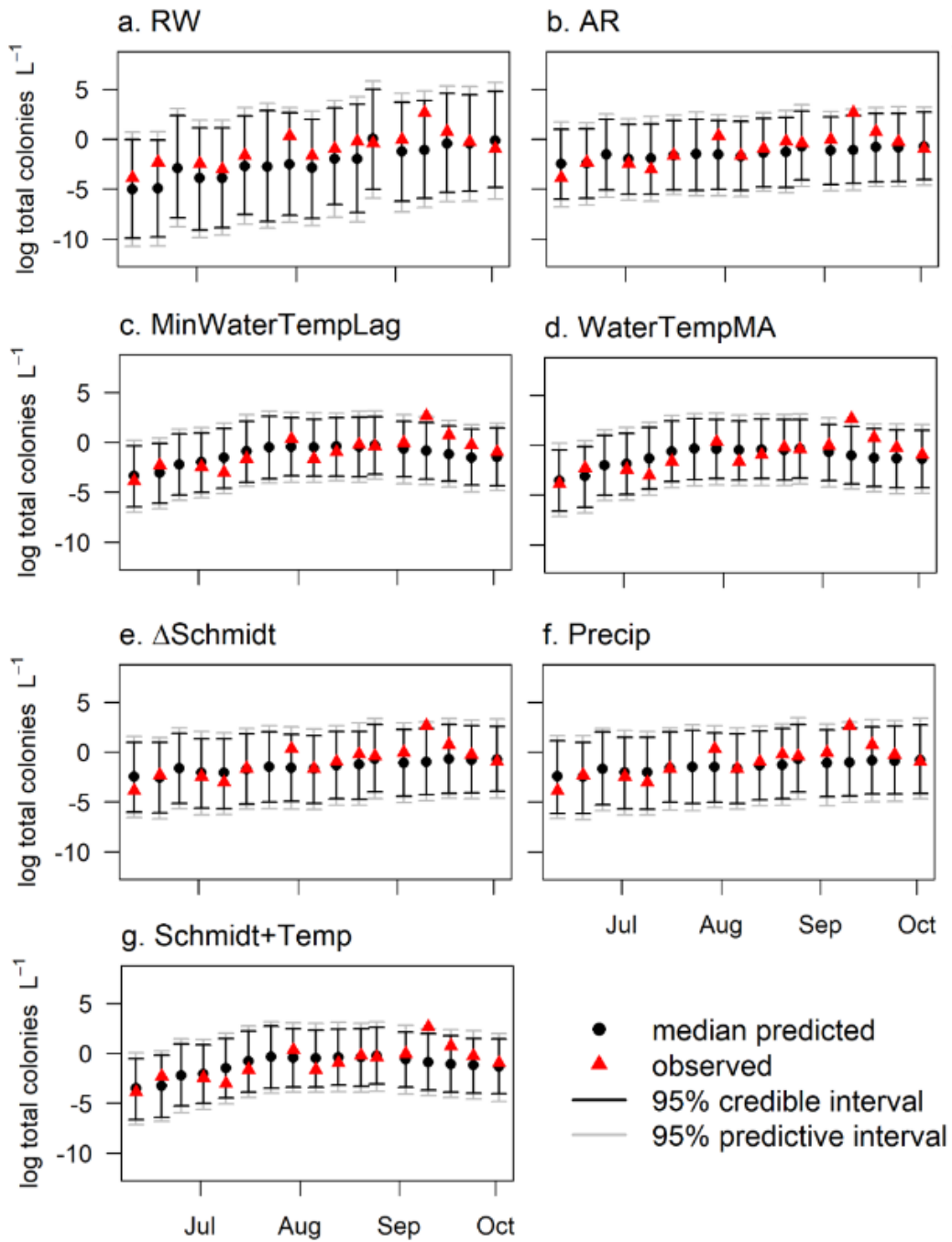
1084 **Figure 5**



1085

1086

1087



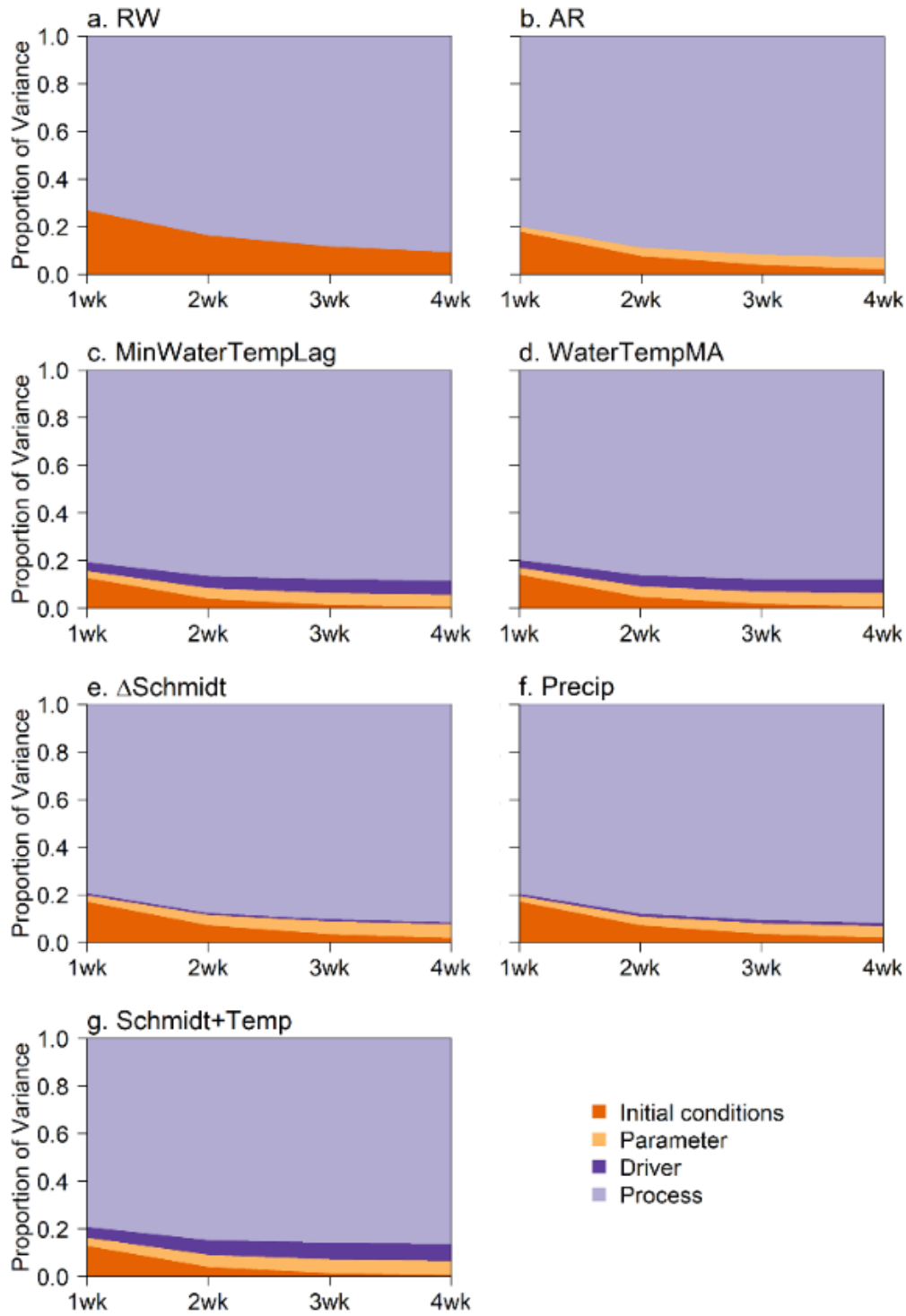
1089

1090

1091

1092

1093 **Figure 7**

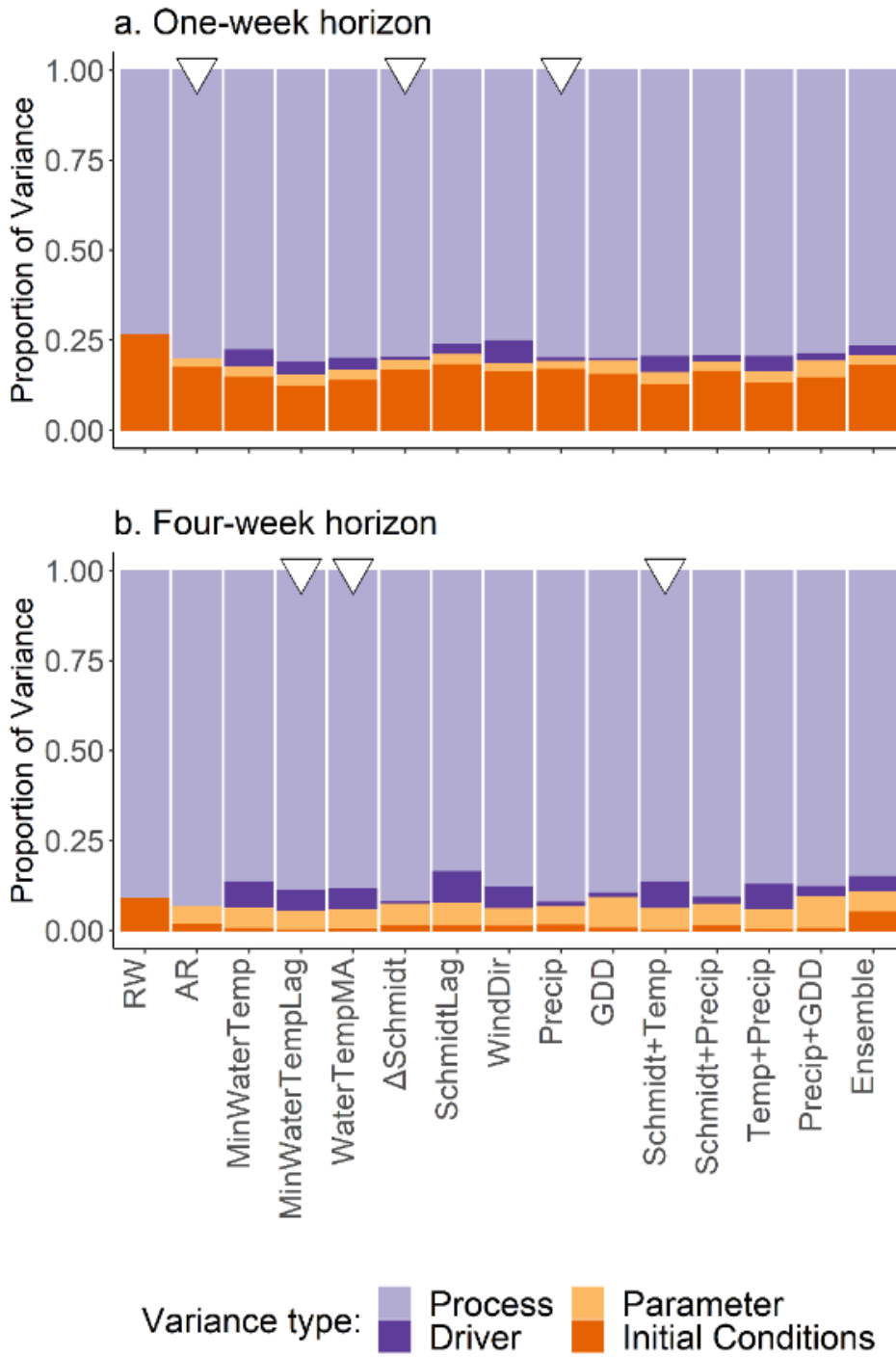


1094

1095

1096

1097 **Figure 8**



1098